

Article

Modified Rime-Ice Growth Optimizer with Polynomial Differential Learning Operator for Single- and Double-Diode PV Parameter Estimation Problem

Sultan Hassan Hakmi ¹, Hashim Alnami ¹, Ghareeb Moustafa ^{1,*} , Ahmed R. Ginidi ² 
and Abdullah M. Shaheen ^{2,*} 

¹ Department of Electrical and Electronic Engineering, College of Engineering and Computer Science, Jazan University, P.O. Box 114, Jazan 45142, Saudi Arabia; shhakmi@jazanu.edu.sa (S.H.H.); halnami@jazanu.edu.sa (H.A.)

² Department of Electrical Engineering, Faculty of Engineering, Suez University, Suez P.O. Box 43221, Egypt; ahmed.ginidi@eng.suezuni.edu.eg

* Correspondence: gmoustafa@jazanu.edu.sa (G.M.); abdullah.mohamed.eng19@suezuni.edu.eg (A.M.S.)

Abstract: A recent optimization algorithm, the Rime Optimization Algorithm (RIME), was developed to efficiently utilize the physical phenomenon of rime-ice growth. It simulates the hard-rime and soft-rime processes, constructing the mechanisms of hard-rime puncture and soft-rime search. In this study, an enhanced version, termed Modified RIME (MRIME), is introduced, integrating a Polynomial Differential Learning Operator (PDLO). The incorporation of PDLO introduces non-linearities to the RIME algorithm, enhancing its adaptability, convergence speed, and global search capability compared to the conventional RIME approach. The proposed MRIME algorithm is designed to identify photovoltaic (PV) module characteristics by considering diverse equivalent circuits, including the One-Diode Model (ONE-DM) and Two-Diode Model TWO-DM, to determine the unspecified parameters of the PV. The MRIME approach is compared to the conventional RIME method using two commercial PV modules, namely the STM6-40/36 module and R.T.C. France cell. The simulation results are juxtaposed with those from contemporary algorithms based on published research. The outcomes related to recent algorithms are also compared with those of the MRIME algorithm in relation to various existing studies. The simulation results indicate that the MRIME algorithm demonstrates substantial improvement rates for the STM6-40/36 module and R.T.C. France cell, achieving 1.16% and 18.45% improvement for the ONE-DM, respectively. For the TWO-DM, it shows significant improvement rates for the two modules, reaching 1.14% and 50.42%, respectively. The MRIME algorithm, in comparison to previously published results, establishes substantial superiority and robustness.

Keywords: RIME optimizer; polynomial differential learning operator; single-diode model; double-diode model; parameter PV cell extraction



Citation: Hakmi, S.H.; Alnami, H.; Moustafa, G.; Ginidi, A.R.; Shaheen, A.M. Modified Rime-Ice Growth Optimizer with Polynomial Differential Learning Operator for Single- and Double-Diode PV Parameter Estimation Problem. *Electronics* **2024**, *13*, 1611. <https://doi.org/10.3390/electronics13091611>

Academic Editor: Cheng Siong Chin

Received: 19 March 2024

Revised: 13 April 2024

Accepted: 17 April 2024

Published: 23 April 2024



Copyright: © 2024 by the authors. Licensee MDPI, Basel, Switzerland. This article is an open access article distributed under the terms and conditions of the Creative Commons Attribution (CC BY) license (<https://creativecommons.org/licenses/by/4.0/>).

1. Introduction

A myriad of countries have noticed an ongoing rise in their energy demand due to their quickly growing populations and aggregate industries. Furthermore, the primary disadvantages of conventional fossil fuel supplies are environmental contamination and fuel shortages. These factors have led scientists to discover a new energy source that may save energy without harming the environment. As a result, scientists have considered using alternate sources of energy that are renewable, such as solar, wind, hydroelectricity, and geothermal power, to produce large amounts of energy without contributing to environmental degradation. Solar PV is one of the sources of clean energy that has attracted a lot of attention in recent decades because of its many benefits, including low maintenance costs, low operating costs, high power density, and low computational costs [1]. PV cells

are arranged in both parallel and series to form the PV panel. The panel output is influenced by the manufacturing process as well as external factors such as light intensity and temperature [2].

Several electrical models have been investigated in the scientific literature, among which are the one-diode model (ONE-DM) [3] and the two-diode model (TWO-DM) [4]. The main challenge is to resolve the nonlinear formula associated with these models and determine the unknown parameters; many approaches of different kinds have been described in the scientific literature [5]. A myriad of approaches to precisely determine the assessment of parameters for PV models could be broadly divided into two categories: analytical techniques and metaheuristics inspired by nature. Examples of analytical techniques are the Lambert W function [6] and the Newton–Raphson method [7]. Nature-inspired metaheuristics (NiMHs) can effectively handle optimization and evaluation problems, since they function like a black box, without imposing any restrictions on the issue formulation. Because of this, NiMH has some advantages over alternative strategies. NiMH finds use in a wide range of industries. Consequently, in order to overcome the parametric problems related to solar PV cell models, academics have recently employed a range of NiMHs [8].

Ridha et al. [9] established an upgraded augmented mutation Harris Hawk Optimizer (AMHHO) to assess the parameters associated with the PV system ground accurately in order to create a more reliable and efficient model. In order to accurately assess the solar cell ground modelling variables, the convergence process of the algorithm can be accelerated by using the proposed method. Chen [10] integrated the adversarial-based exploration method and chaotic drift strategy into the Harris Hawk Optimizer (HHO). In order to boost global convergence and local mining capabilities, the moth flame method (MFO) was demonstrated in [11], to identify the parameters of PV modules. This led to outstanding outcomes in the ONE-DM and TWO-DM PV models.

An Improved Sine Cosine Algorithm called ISCA was proposed by Chen et al. [12] to evaluate the unknown parameters for the ONE-DM and TWO-DM. Wu [13] proposed a method for parameter evaluation based on the improved ant-lion optimizer (IALO). IALO achieved favorable results using the photovoltaic model. Liu et al. [14] employed the upgraded Harris Hawk algorithm (CCNMHHO) to ascertain the parameters of the solar model. Merchaoui proposed the adaptive variational Particle Swarm Optimization (PSO) approach for identifying the unknown parameters of different photovoltaic models and maximizing the ideal parameters for solar models under diverse conditions [15,16]. Jiao et al. [17] used orthogonal learning (OL) and generalized opposition-based learning (GOBL) approaches to accurately and efficiently evaluate the characteristics of PV modules' solar cells. Abbassi et al. [18] proposed an improved algorithm based on the salp swarm method that makes use of an opposition-based learning strategy to tackle the parameter estimation issue encountered by solar cells. Ridha et al. [19] provided a thorough analysis based on multi-objective optimization and multi-criteria approaches on independent PV systems in order to help select the optimal design solutions. The metaheuristic technique and its variants have several drawbacks, even if its execution is faster and with higher solution quality. Furthermore, the approach is a somewhat specialized, and its excellent performance is restricted to particular kinds of optimization problems, which limits its use cases.

Studying PV systems is crucial due to their pivotal role as ideal companions for both renewable and traditional energy sources in hybrid energy systems. These systems are widely adopted globally because of their reliability and stability in energy production from individual sources; such systems include PV/Grid [20], PV energy forecasting [21], PV/STATCOM [22], PV/Voltage regulators [23], and microgrid management [24]. Additionally, a variety of maximum power point tracking (MPPT) methodologies have been developed to optimize the operation of solar PV arrays for maximum power output [25]. In Ref. [26], a global MPPT-based variable vortex search (VVS) methodology was presented for photovoltaic (PV) generation systems. In this study, several modern heuristic algorithms were utilized and statistically analyzed via the Monte Carlo method under partial

shading conditions (PSCs). In Ref. [27], several techniques were contrasted and adopted for MPPT, including Perturb and Observe (P&O), cuckoo search, Jaya, Salp swarm, Emperor Penguin optimization, Grey Wolf optimization, and artificial Bee colony and Ant colony optimization algorithms, while a Chimp Optimization algorithm (ChOA) was utilized and simulated for the same purpose via MATLAB 2017b/SIMULINK in Ref. [28].

Recently, the Rime Optimization Algorithm (RIME) method was introduced by H. Su et al. [29]. By inspiring the natural development of soft and hard rime particles. Rime agents experience Soft-Rime Search (SRS) and Hard-Rime Puncture (HRP) phases to simulate environmental conditions. Parameters such as adhesion degree and attachment coefficient impact particle distance, thereby influencing condensation probability and optimizing the process. Also, fitness values act as guides for information exchange between agents. In recent times, novel domains have surfaced in the utilization of fractional differential systems, particularly leveraging their inherent advantages in viscoelasticity [30–33]. This paper proposes a Modified RIME (MRIME) incorporating a Polynomial Differential Learning Operator (PDLO). The proposed incorporation of PDLO with the presented MRIME algorithm introduces diversity in the population by combining information from two randomly selected individuals to update the position of the current individual. The randomness introduced by the permutation helps in exploring the search space effectively. The proposed MRIME algorithm is designed to identify PV module characteristics by considering diverse equivalent circuits, including the ONE-DM and TWO-DM, to determine the unspecified parameters of the PV. To showcase the effectiveness of the MRIME algorithm, it undergoes testing against more advanced algorithms in the context of the PV ONE-DM and TWO-DM. The experimental study illustrates the excellent outcomes achieved by the proposed MRIME algorithm. In summary, the key contributions of this paper are as follows:

- An enhanced MRIME algorithm is proposed by incorporating the PDLO to enhance its searching diversity.
- The proposed MRIME algorithm is implemented on two commercial PV systems of the STM6-40/36 module and R.T.C. France cell.
- The MRIME algorithm exhibits considerable advantages and robustness for both PV models compared to the conventional RIME algorithm and previously reported outcomes.
- Tests of the MRIME algorithm's efficacy on the PV ONE-DM and TWO-DM reveal a very good correlation between simulated and actual data.

The remaining structure of this paper is as follows: Section 2 presents the problem definition, considering the ONE-DM and TWO-DM frameworks. Section 3 thoroughly describes the proposed MRIME technique. Experimental findings are examined in detail in Section 4, confirming the effectiveness of the MRIME technique. Section 5 presents the conclusions for this work.

2. Problem Formulation of Solar PV Parameter Extraction

This section covers the ONE-DM and TWO-DM for mathematical simulation of PV modules [22]. Following that, the objective function will be highlighted in order to address the problem of parameter estimation for the aforementioned PV models.

2.1. ONE-DM

The ONE-DM, represented in Figure 1 [34], is simple to create when the solar cell is thought of as an inner parallel circuit. The entire output current of the circuit is indicated by the symbol (I), which may be expressed using the following formula [35]:

$$I = I_{ph} - I_{sh} - I_{d1}, \quad (1)$$

where I_{ph} stands for the photocurrent, I_{sh} is the shunt resistor current, and I_d is the diode current.

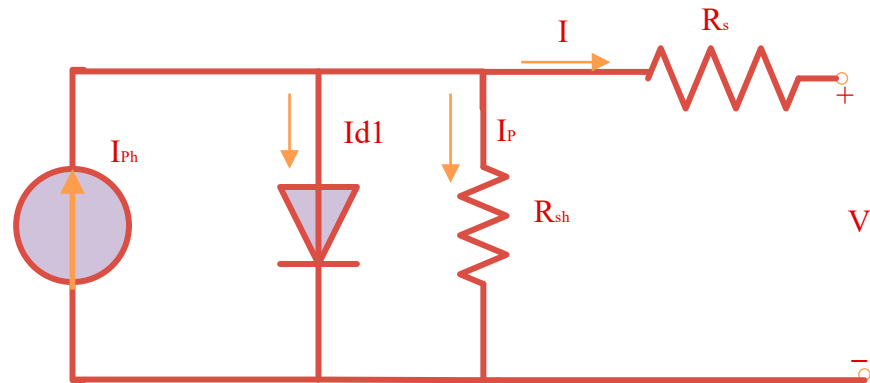


Figure 1. Demonstration of ONE-DM circuit.

The shunt resistor current (I_{sh}) may be expressed using the following formula [36]:

$$I_{sh} = \frac{I \cdot R_s + V}{R_{sh}}, \tag{2}$$

where V denotes the output voltage, and R_s and R_{sh} stand for the series and shunt resistances. The diode current is represented mathematically by I_{d1} , which may be computed [37] by applying Equation (3).

$$I_{d1} = I_{s1} \left[\exp\left(\frac{I \cdot R_s + V}{\eta_1 \cdot V_{thr}}\right) - 1 \right], \tag{3}$$

where I_{s1} denotes the diode reverse saturation current and η_1 indicates the ideal factor for the diode. The junction thermal voltage (V_{thr}) [38] is determined by Equation (4).

$$V_{thr} = \frac{K_B \cdot T}{q_c}, \tag{4}$$

where T signifies the temperature defined in Kelvin, q_c denotes the electron charge of $1.60217646 \times 10^{-19}$ C, and K_B indicates the Boltzmann's value (1.380653×10^{-23} J/K). Finally, by combining the aforementioned formulations, Equation (5) explains the link between various parameters with the output current [39].

$$I = I_{ph} - I_{s1} \times \left[\exp\left(\frac{I \cdot R_s + V}{\eta_1 \cdot V_{thr}}\right) - 1 \right] - \frac{V}{R_{sh}} - \frac{I \cdot R_s}{R_{sh}}, \tag{5}$$

Five variables (R_{sh} , R_s , I_{s1} , I_{ph} , and η_1) need to be extracted in the ONE-DM, as can be determined in Equation (7).

2.2. TWO-DM

The loss of composite currents throughout the ONE-DM is addressed by the development of the TWO-DM. Consequently, the computation of the overall current flow in the equivalent circuit displayed in Figure 2 is indicated by Equation (6).

$$I = I_{ph} - I_{sh} - I_{d1} - I_{d2}, \tag{6}$$

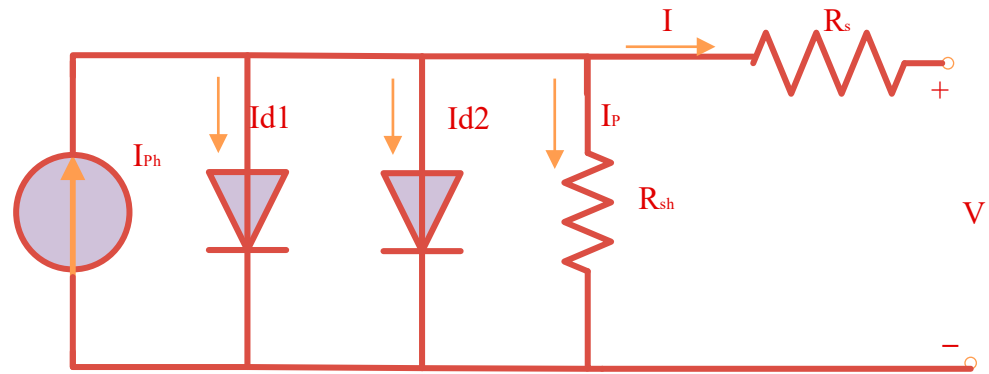


Figure 2. Demonstration of the TWO-DM circuit.

By integrating the aforementioned formulations, Equation (7) establishes a correlation between the current flowing through the output, the output voltage, and multiple other variables in the TWO-DM [38]:

$$I = I_{ph} - I_{s1} \left[\exp \left(\frac{I \cdot R_s + V}{\eta_1 \cdot V_{thr}} \right) - 1 \right] - I_{s2} \left[\exp \left(\frac{I \cdot R_s + V}{\eta_2 \cdot V_{thr}} \right) - 1 \right] - \frac{V}{R_{sh}} - \frac{I \cdot R_s}{R_{sh}}, \quad (7)$$

where I_{s1} and I_{s2} denote the first and second diode reverse saturation currents, while η_1 and η_2 indicate the ideal factor for the two diodes.

Seven variables (I_{s1} , R_{sh} , R_s , I_{s2} , I_{ph} , η_1 , and η_2) need to be extracted in the TWO-DM, as can be determined using Equation (7).

2.3. PV Module Development

The PV module model has a more intricate design; it is primarily made up of several solar cells coupled in parallel or series. The current flowing [40] as the output displayed in the PV module model’s equivalent circuit can be addressed by observing Equation (8).

$$I = N_p \left(\begin{array}{l} I_{ph} - I_{s1} \left[\exp \left(\frac{1}{\eta_1 \cdot V_{th} \cdot N_s} \cdot ((V + I \cdot R_s \cdot N_s) / N_p) \right) - 1 \right] \\ - I_{s2} \left[\exp \left(\frac{1}{\eta_2 \cdot V_{th} \cdot N_s} \cdot ((V + I \cdot R_s \cdot N_s) / N_p) \right) - 1 \right] \\ - I_{s3} \left[\exp \left(\frac{1}{\eta_3 \cdot V_{th} \cdot N_s} \cdot ((V + I \cdot R_s \cdot N_s) / N_p) \right) - 1 \right] \end{array} \right) - ((V + I \cdot R_s \cdot N_s) / N_p) \cdot \frac{1}{N_p \cdot N_s \cdot R_{sh}}, \quad (8)$$

where the numbers of solar cells in parallel and series are indicated by N_p and N_s , respectively.

2.4. Objective Model

To establish objective functions that are suitable for a number of computational methods, it must first be possible to quantify the output voltage and current that is produced in each of the models [41–43]. As a result, the function’s target may be to find the disparity between the current that is generated in the model that has been developed and the experimental current. The present research aims to decrease the RMSE, which is defined as follows:

$$RMSE = \sqrt{\frac{1}{P \cdot N} \left(\sum_{K=1}^{PN} (I_{cal}^K(V_{exp}^K, x) - I_{exp}^K)^2 \right)}, \quad (9)$$

where PN denotes the number of measured data points, and I_{exp}^K and V_{exp}^K stand for the observed current and voltage. In addition, the PV determination characteristic problem—which has to do with discovering a solution in the solution space that lessens the objective function—is revealed by the form of (x) .

3. MRIME Algorithm for PV Parameter Estimation

The RIME algorithm draws inspiration from natural processes, specifically the growth of soft and hard rime particles, to design its optimization strategy. The positions of rime agents, or particles, represent the solution vectors in the search space. It mimics the associated environmental conditions in two phases: the Soft-Rime Search (SRS) and Hard-Rime Puncture (HRP) [29]. It requires several key steps to perform optimization, as follows.

3.1. Rime Initialization Phase

The population is initialized with Nm rime agents, each represented as a rime particle with D dimensions. A random search is employed in the initialization process to determine the positions of rime agents in the search space.

Consequently, the population of rime agents, denoted as R_{POP} , is succinctly expressed using the positions of individual rime particles, represented by $Rm_{i,j}$ in Equation (10).

$$R_{POP} = [Rm_{i,j}]_{Nm \times D} = \begin{bmatrix} Rm_{1,j} \\ Rm_{2,j} \\ \cdot \\ \cdot \\ Rm_{Nm,j} \end{bmatrix}_{i=1:D} = \begin{bmatrix} Rm_{1,1} & Rm_{1,2} & \dots & \dots & Rm_{1,D} \\ Rm_{2,1} & Rm_{2,2} & \dots & \dots & Rm_{2,D} \\ \cdot & \cdot & \dots & \dots & \cdot \\ \cdot & \cdot & \dots & \dots & \cdot \\ Rm_{Nm,1} & Rm_{Nm,2} & \dots & \dots & Rm_{Nm,D} \end{bmatrix}, \quad (10)$$

where R_{POP} is the population matrix, which consists of the vectors of the rime agents ($Nm \times 1$), and each rime agent vector consists of several design parameters ($1 \times D$).

These positions are subject to limits, with upper (Up_j) and lower (Lo_j) boundaries defining the permissible range for each dimension. Adopting a conventional approach observed in many population-based algorithms, the rime population undergoes initialization through a random search process during the initial phase. The resulting expression for the position $Rm_{i,j}$ during this initialization is detailed below.

$$Rm_{ij} = Lo_j + rd_1 \cdot (Up_j - Lo_j), \quad i = 1 : Nm, \quad j = 1 : D, \quad (11)$$

where rd_1 is a randomly selected number inside the range $[0, 1]$.

3.2. SRS Phase

The algorithm simulates the freezing of rime particles on the surface of an object, mimicking the soft-rime growth process. Rime agents move in the search space with the influence of wind force and their own randomness, ensuring broad coverage in the early iterations. The position update of rime agents is determined using a formula that includes the best rime agent’s position, environmental factors, and randomness, as follows:

$$Rm_{ij}^* = Rm_{best,j} + rd_2 \cdot \beta \cdot \cos(\theta) \cdot [AD \cdot (Up_j - Lo_j) + Lo_j], \quad \text{if } rd_3 < E, \quad (12)$$

where the degree of adhesion (“ AD ”) characterizes the proximity between the best rime agent and a randomly chosen rime agent, with “ AD ” constrained within the range $[0, 1]$. The modified position of the rime agent i in the dimension j at the iteration after the SRS phase, denoted by Rm_{ij}^* , is determined based on the position of the best rime agent in the population ($Rm_{best,j}$). The directional control is governed by the interplay of “ rd_2 ” and “ $\cos(\theta)$ ”, where “ rd_2 ” is a random number in the range $[-1, 1]$. Also, “ rd_3 ” is a random number in the range $[0, 1]$, while θ is defined in Equation (13).

$$\theta = \left(\frac{It}{It^{max}} \right) \cdot \left(\frac{\pi}{10} \right), \quad (13)$$

In this context, the symbol “ It ” denotes the iteration count index, while “ It^{max} ” represents the total number of iterations.

The environmental factor, represented by “ β ”, models external conditions and ensures the convergence of the rime population, as specified in Equation (14).

$$\beta = 1 - \frac{1}{\omega} \cdot \left(\text{round} \left(\frac{\omega \cdot It}{It^{\max}} \right) \right), \quad (14)$$

The function “*round*” is employed to round numerical values, and the parameter “ ω ” is introduced to regulate the segmentation of the step function, with a default value of 5 as per [29].

Additionally, the variable “ rd_3 ” is a random number within [0, 1], and “ E ” signifies the attachment coefficient, influencing the coalescence probability of the rime agent. The attachment coefficient gradually increases throughout the search process, as follows:

$$E = \left(\frac{It}{It_{Max}} \right)^{1/2}, \quad (15)$$

3.3. HRP Phase

In strong wind conditions, the algorithm emulates the simpler and more regular growth of hard-rime particles. The HRP mechanism facilitates information exchange between agents to improve convergence and escape local optima, as follows:

$$Rm_{newij} = \begin{cases} Rm_{best,j} & rd_4 < Fit^n(Rm_i) \\ Rm_{ij}^* & Else \end{cases}; \quad i = 1 : Nm, \quad j = 1 : D, \quad (16)$$

where Rm_{newij} indicates the newly created position of the rime agent i in the dimension j , while “ rd_4 ” is a random number within [0, 1]. As shown, the positions of rime agents are updated based on the fitness values and normalized fitness values ($Fit^n(Rm_i)$), promoting crossover between agents, where

$$Fit^n(Rm_i) = \frac{Fit(Rm_i)}{\sqrt{\sum_{i=1}^{Nm} (Fit(Rm_i))^2}}, \quad (17)$$

where $Fit^n(Rm_i)$ is the value of the fitness function regarding the current position of the rime agent i .

3.4. Proposed PDLO Incorporation

In this paper, the PDLO is incorporated to enhance the searching capabilities and diversity of the RIME algorithm. The PDLO is commonly used in differential evolution (DE) algorithms for optimization [44]. This operator enhances population diversity by merging information from two randomly chosen individuals to update the current rime particle’s position. PDLO, an extension of DE, adapts the mutation strategy to amplify exploration and exploitation within the search space. The mutation formula in PDLO incorporates a polynomial function, injecting non-linear characteristics into the mutation operation. To execute the integrated PDLO, two random integers ($index1$ and $index2$) are drawn from the population. Subsequently, the newly derived position of rime agent i can be formulated as follows:

$$Rm_{newi} = Rm_i + \phi \cdot (Rm_{index1} - Rm_{index2}), \quad i = 1 : Nm, \quad (18)$$

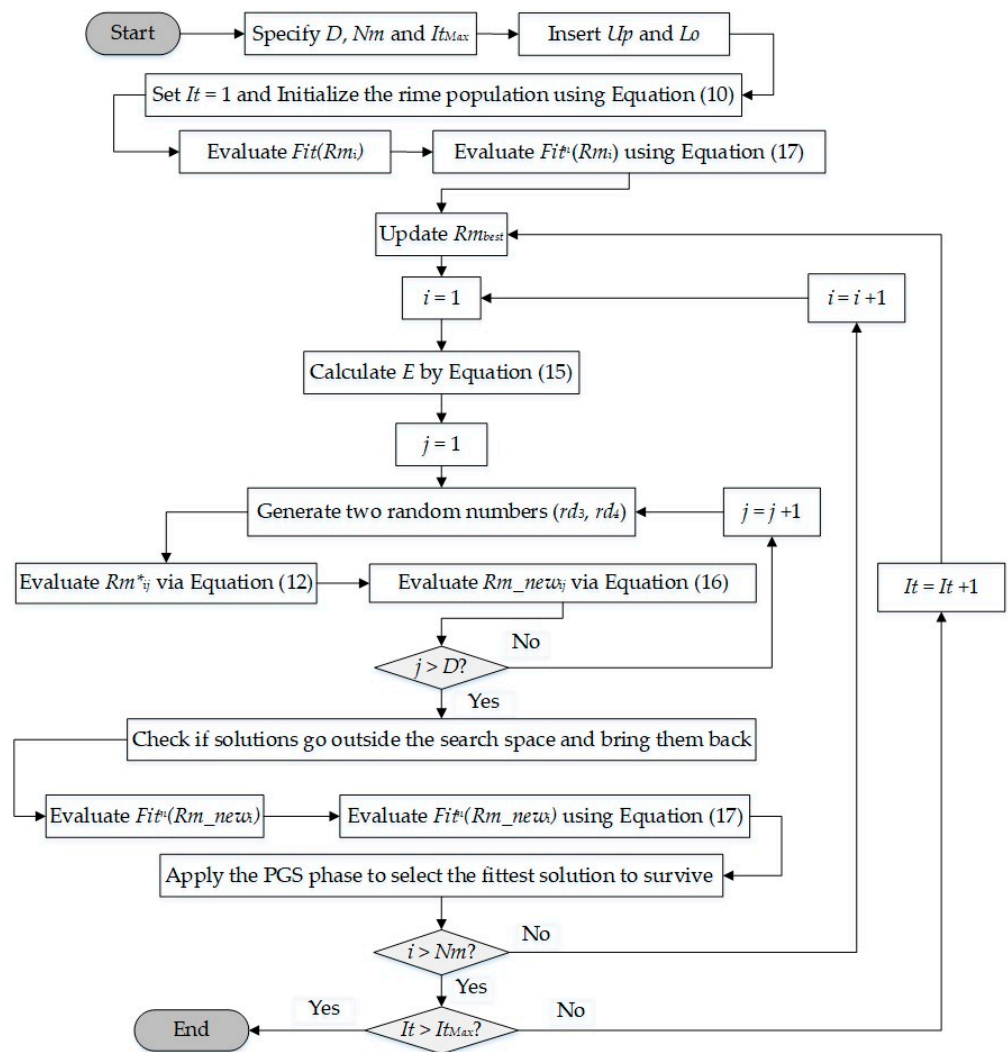
where ϕ is a generated random number between 0 and 1. Thus, the update involves the weighted sum of the difference between two randomly selected elements (Rm_{index1} and Rm_{index2}), while the weight ϕ controls the contribution of this difference to the update.

3.5. Positive Greedy Selection (PGS) Phase

After generating the new positions of the rime particles by the HRP-SRS phases (Equations (12) and (16)) or the PDLO (Equation (18)), the PGS mechanism is employed to compare fitness values before and after the update. If the updated fitness value is better, the suboptimal solution is replaced with the optimal one, enhancing the global solution quality. This mechanism actively replaces agents during updates, to ensure a more optimal population evolution.

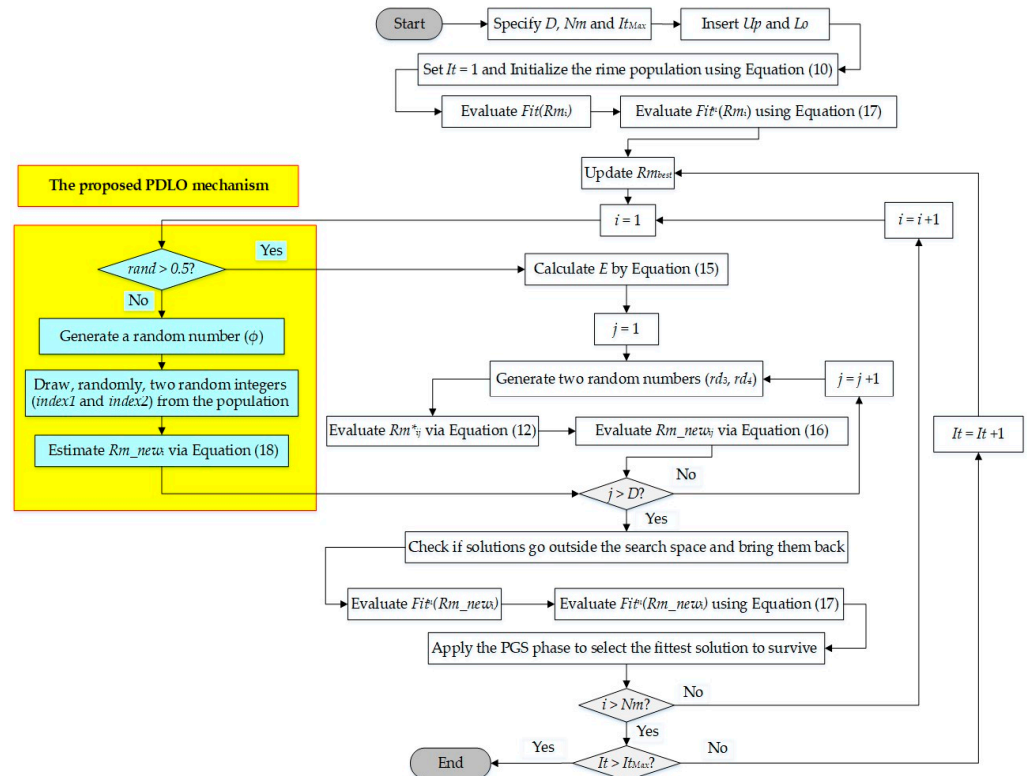
3.6. Iterative Process

Figure 3a,b displays the main steps of the standard RIME against the proposed MRIME optimizer, where the entire process is iteratively performed until a predefined number of iterations (It_{Max}) is reached. At each iteration, the proposed MRIME updates the positions of rime agents utilizing the SRS and the HRP phases or the PDLO mechanism, evaluates fitness values, and performs PGS. In the proposed MRIME algorithm with PDLO, the inclusion of a polynomial function enables fine-tuned control over the impact of each mutation vector component, contributing flexibility to the exploration process. The introduction of randomness through permutation and the variables adds effectiveness to the exploration of the search space. The optimal rime agent in the swarm, determined by the best fitness value, is output as the solution to the optimization problem.



(a) The standard RIME optimizer.

Figure 3. Cont.



(b) The proposed MRIME optimizer.

Figure 3. Main steps of the standard RIME and the proposed MRIME optimizers.

4. Simulation Results

In this section, the proposed MRIME algorithm, along with the conventional RIME algorithm, is expanded to estimate PV parameters for two distinct commercial systems—R.T.C. France and STM6-40/36. The R.T.C. France cell is a commercially available silicon cell operating at 1000 W/m² sun irradiance and a temperature of 33 degrees Celsius. The second module, STM6-40/36, consists of 36 monocrystalline cells linked in series, each with dimensions of 38 mm × 128 mm, operating at 51 °C and an irradiation of 1000 W/m² [45].

For both PV systems, two cases are explored, involving different equivalent circuits: ONE-DM (Case 1) and TWO-DM (Case 2). In both algorithms, a population of one hundred rime particles is considered, with a maximum limit of one thousand iterations. Additionally, each technique undergoes twenty different running times for comprehensive analysis.

4.1. First Test Investigation: R.T.C. France Cell

4.1.1. Case 1: ONE-DM

In the current case, the ONE-DM characteristics of the R.T.C. France cell are extracted using the suggested MRIME and the RIME. Table 1 lists the five unknown ONE-DM parameters for which the experiment’s best outcomes were obtained for every approach. The results show that the suggested MRIME outperforms the RIME and comparator approaches in terms of competitiveness. This means that the regular RIME obtained an RMSE of 9.9755×10^{-4} , whereas the MRIME obtained the best RMSE value of 9.8602×10^{-4} . Additionally, the PV-derived electrical parameters utilizing the reported optimization approaches are displayed in the table; these include the Classified perturbation mutation PSO (CPMPSO) [46], HEAP Optimizer [47], multi-verse optimizer (MVO) [48], Lightning Attachment Procedure Optimization (LAPO) [49], particle swarm optimization (PSO) [50], Enhanced MPA (EMPA) [47], neighborhood scheme-based Laplacian MBA (NLBMA) [51], a performance-guided JAYA (PGJAYA) [52], Forensic-Based Investigation Optimizer (FBI) [53], Barnacles Mating Optimizer (BMA) [54], Enriched Harris Hawks optimization (EHHO) [10], Jellyfish Search (JFS) Optimizer [47], Ant Lion Opti-

mizer (ALO) [55], Growth optimizer GO [38], flexible PSO (FPSO) [3], Hybrid Firefly and Pattern Search (HFAPS) [56], Equilibrium Optimizer (EO) [47], hybrid PSO–GWO algorithm (PSOGWO) [57], and Marine Predator Algorithm (MPA) [47]. Moreover, the table specifies the assessed parameters of (MRIME and RIME), which are (57.37254497 Ω and 53.71865291 Ω), (0.760557 A and 0.760776 A), (1.485377 and 1.481184), (0.036257632 Ω and 0.036377096 Ω), and (3.36869×10^{-1} μA and 3.23021×10^{-1} μA) for the shunt resistance, photo-current, ideality factor for d1, series resistance, and saturation current for d1, respectively. Additionally, electrical variables acquired using various inspirational optimizers are expressed in this table.

Table 1. Extracted PV cell parameters based on MRIME versus RIME and other reported methods applied for the ONE-DM of the R.T.C. France cell.

Algorithm	I_{ph} (A)	I_{sd} (μA)	n	R_{sh} (Ω)	R_s (Ω)	RMSE
MRIME	0.760557	3.36869×10^{-1}	1.485377	57.37254497	0.036257632	9.8602×10^{-4}
RIME	0.760776	3.23021×10^{-1}	1.481184	53.71865291	0.036377096	9.9755×10^{-4}
MPA [47]	8.184927	7.94459×10^{-2}	1.285180059	92.14823504	0.004537611	1.487×10^{-2}
FBI [53]	8.217030039	2.72156×10^{-2}	1.215208065	6.235899986	0.004814219	9.88×10^{-4}
JFS [47]	8.193182	4.72×10^{-2}	1.250052	14.97462	0.004679	9.477×10^{-3}
PGJAYA [52]	8.2167	0.002284	58.1742	773.8117	0.3435	1.5455×10^{-4}
EO [47]	8.209153	2.85×10^{-2}	1.218068	7.714703	0.004815	2.888×10^{-3}
CPMPSO [46]	8.21689146	0.00224195	1.07641028	763.535149	0.34381405	1.53903×10^{-3}
FPSO [3]	8.2186	0.001436	56.9854	130.2813	0.2409	2.8214×10^{-2}
GO [38]	8.192967	4.31808×10^{-2}	1.244346	15.103921	0.004710	8.515347×10^{-3}
HFAPS [56]	8.1992	0.154161	74.5795	1448.2590	0.2396	4.9863×10^{-2}
EHHO [10]	8.2224	0.000001	80.6915	1806.0252	0.1835	5.9507×10^{-2}
PSO [50]	8.2027	2.8852	1.6052	33.8855	0.0019	1.0195×10^{-1}
PSOGWO [57]	8.2132	9.6768	1.7463	38.8968	0.0011	1.2700×10^{-1}
MVO [48]	8.2527	0.063908	69.2388	134.4813	0.1341	8.3800×10^{-2}
BMA [54]	8.1950	3.1015	1.6130	100.0000	0.0019	1.0244×10^{-1}
LAPO [49]	8.2155	8.1491	1.7258	5.0000	0.001	1.3813×10^{-1}
EMPA [47]	8.21195	3.59×10^{-2}	1.232551	7.560713	0.004742	3.847×10^{-3}
NLBMA [51]	8.1467	0.0022	1.0839	5.0000	0.0045	3.3610×10^{-2}
HEAP [47]	8.200974	4.49×10^{-2}	1.246924	11.87468	0.004696	7.425×10^{-3}

The corresponding convergence lines can be seen in Figure 4. The MRIME converged extremely quickly in the first 60 iterations, as depicted in this figure, demonstrating the MRIME's excellent convergence capacity. Additionally, Figure 5 shows the twenty obtained RMSE objectives for Case 1's RIME and MRIME. This figure illustrates that the RMSE of RIME is between [9.9755×10^{-4} and 2.5096×10^{-3}], but the RMSE of MRIME is between [9.8602×10^{-4} and 1.0035×10^{-3}]. It can be established from the figure that the enhancements of the MRIME approach are 30.878%, 1.156%, 46.525%, and 99.634%, respectively, when compared to the mean, best, worst, and standard deviation of the outcomes of the RIME techniques. These results corroborate the superiority of the developed MRIME for the ONE-DM of the R.T.C. France cell. Consequently, the suggested MRIME yielded the highest value, indicating that MRIME outperforms RIME in terms of stability, accuracy, and efficacy when determining ONE-DM parameters through comparison. It is reliable that the MRIME identified the validity with the ONE-DM.

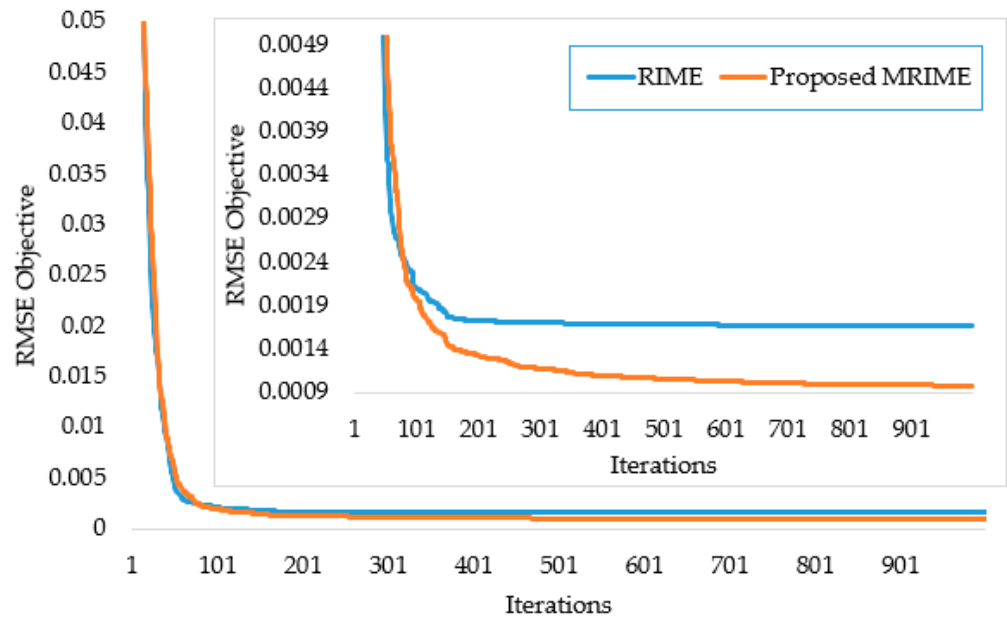


Figure 4. Convergence lines of RIME and MRIME for the ONE-DM of the R.T.C. France cell.

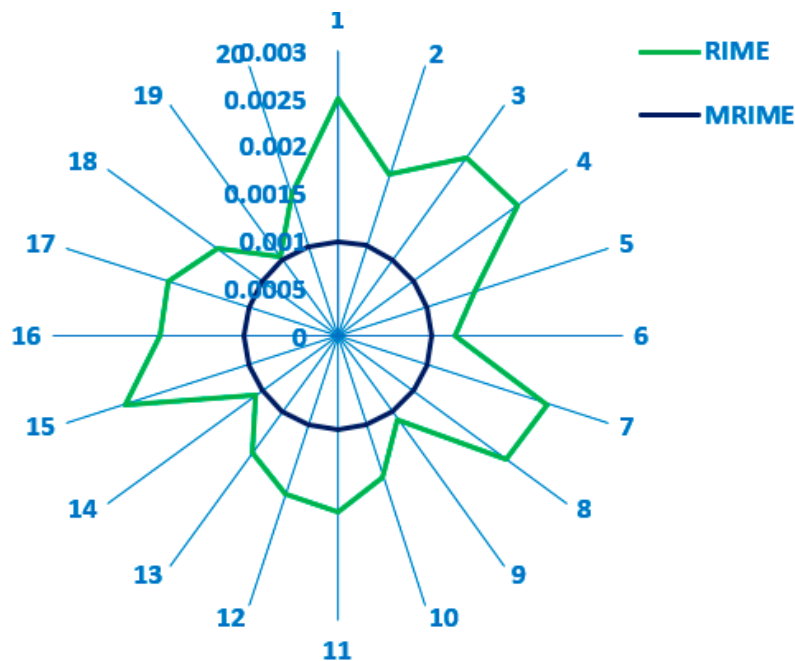


Figure 5. RIME and MRIME of the twenty obtained RMSE objectives for the ONE-DM of the R.T.C. France cell.

For the ONE-DM, the simulated and measured I-V and P-V characteristics are shown in Figure 6a,b. It can be proven that the data created by the MRIME technique are almost the same as the data obtained through experimentation, indicating that the MRIME technique proved effective in obtaining the power and current with diverse voltage levels. As illustrated in Figure 7a,b, the absolute errors between the simulated and measured currents are between 2.85343×10^{-9} and 6.24849×10^{-6} , whereas the absolute error between the simulated and measured powers is between 1.95909×10^{-6} and 1.4581×10^{-3} .

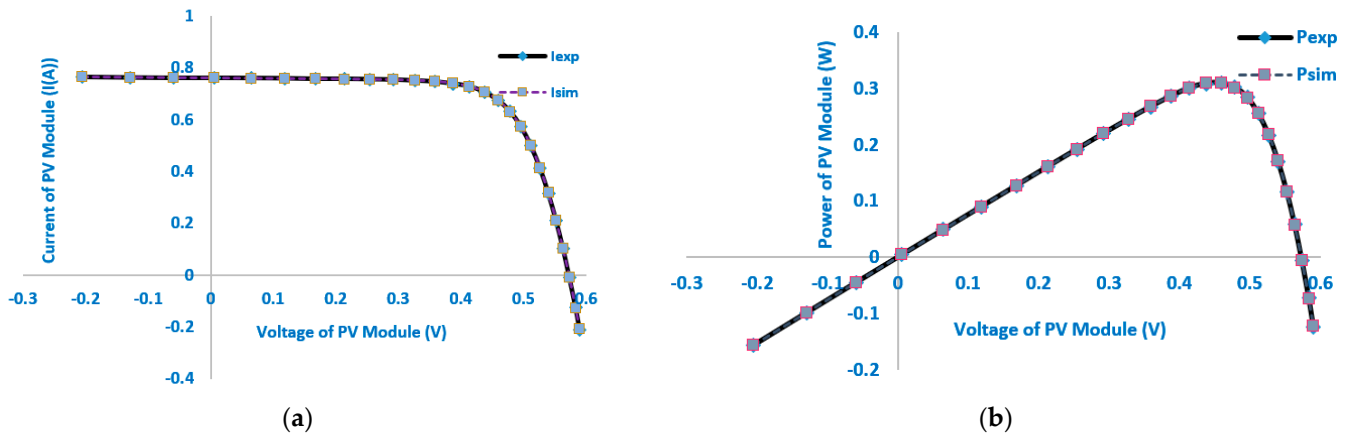
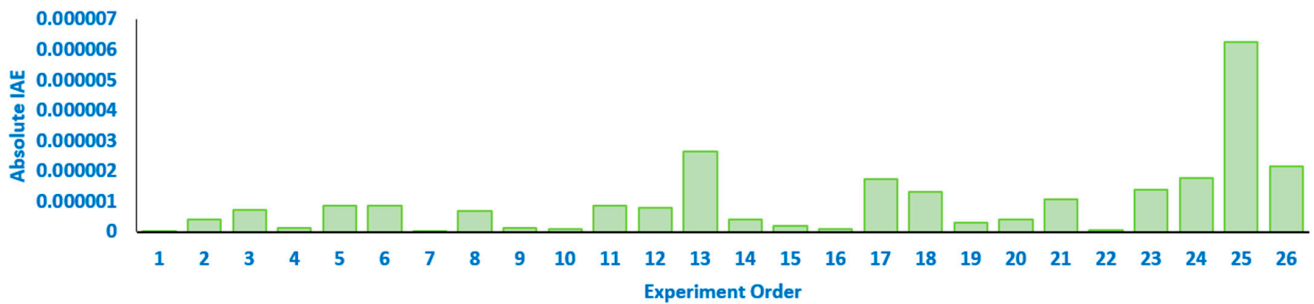
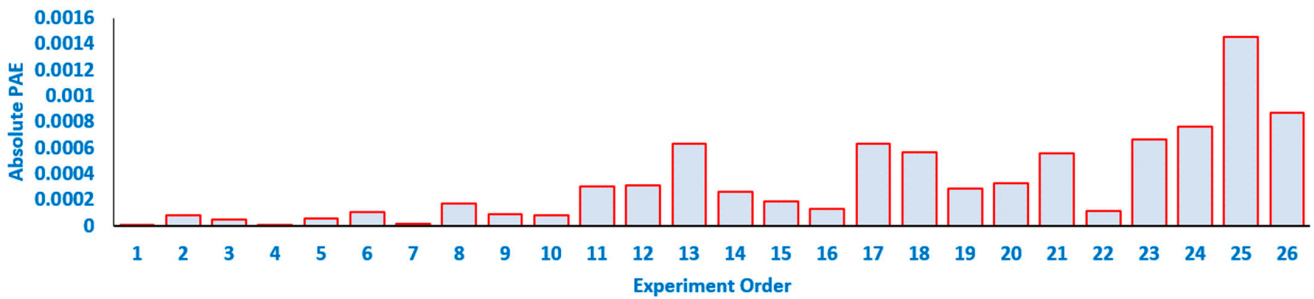


Figure 6. (a) I-V and (b) P-V characteristics of the proposed MRIME for the ONE-DM of the R.T.C. France cell.



(a) Currents Absolute Errors



(b) Powers Absolute Errors

Figure 7. The absolute errors between the simulated and measured currents and powers concerning the MRIME for the ONE-DM of the R.T.C. France cell.

4.1.2. Case 2: TWO-DM

In the current case, the TWO-DM characteristics of the R.T.C. France cell are extracted using the suggested MRIME and the RIME. Table 2 lists the seven unknown TWO-DM parameters for which the experiment’s best outcomes were obtained for every approach. The results show that the suggested MRIME outperforms the RIME and comparator approaches in terms of competitiveness. This means that the regular RIME obtained an RMSE of 9.9382×10^{-4} , whereas the MRIME obtained the best RMSE value of 9.8251×10^{-4} . Moreover, the table specifies the assessed parameters of (MRIME and RIME), which are (55.64800559 Ω and 53.58354831 Ω), (0.760780758 A and 0.760864277 A), (1.999974446 and 1.827202939), (1.482783518 and 1.448694376), (0.036767981 Ω and 0.036173672 Ω), (8.0438×10^{-7} A and 4.3113×10^{-8} A), and (2.19744×10^{-7} A and 3.25421×10^{-7} A) for the shunt resistance, photo-current, ideality factor for d1, ideality factor for d2, series resistance, saturation current for d1, and saturation current for d2, respectively.

Table 2. Electrical parameters of the proposed MRIME and the standard RIME for the TWO-DM of the R.T.C. France cell.

Applied Algorithm	RIME	MRIME
I_{Ph} (A)	0.760864277	0.760780758
R_s (Ω)	0.036173672	0.036767981
R_{Sh} (Ω)	53.58354831	55.64800559
I_{S1} (A)	4.3113×10^{-8}	8.0438×10^{-7}
η_1	1.827202939	1.999974446
I_{S2} (A)	3.25421×10^{-7}	2.19744×10^{-7}
η_2	1.482783518	1.448694376
RMSE	9.9382×10^{-4}	9.8251×10^{-4}

Table 3 presents a comparison between the proposed MRIME technique and both the standard RIME and various optimization tools for the TWO-DM system that have been documented in literature, such as the flower pollination algorithm [58], teaching–learning–based ABC [59], TLBO [60], ABC [61], Cat Swarm Algorithm (CSA) [62], SCA [12], and generalized oppositional TLBO [4]. It is demonstrated that the proposed MRIME technique outperforms other approaches in obtaining the lowest RMSE.

Table 3. Comparative assessment between the proposed MRIME technique and various optimization tools for the TWO-DM of the R.T.C. France cell.

Algorithms	RMSE
MRIME	9.8251×10^{-4}
RIME	9.9382×10^{-4}
ABC [61]	1.28482×10^{-3}
Teaching–learning–based ABC [59]	1.50482×10^{-3}
Generalized oppositional TLBO [4]	4.43212×10^{-3}
TLBO [60]	1.52057×10^{-3}
CSA [62]	1.22×10^{-3}
SCA [12]	9.86863×10^{-4}
Flower pollination algorithm [58]	1.934336×10^{-3}

The corresponding convergence lines can be seen in Figure 8. The MRIME converged extremely quickly in the first 50 iterations, as depicted in this figure, demonstrating the MRIME’s excellent convergence capacity. Additionally, Figure 9 shows the thirty obtained RMSE objectives for Case 1’s RIME and MRIME. This figure illustrates that the RMSE of RIME is between [9.9382×10^{-4} and 3.1870×10^{-3}], but the RMSE of MRIME is between [9.8251×10^{-4} and 1.0135×10^{-3}]. It can be established from the figure that the enhancements of the MRIME approach are 45.3824%, 1.1379%, 68.1989%, and 99.0358%, respectively, when compared to the mean, best, worst, and standard deviation of the outcomes of the RIME techniques. These results corroborate the superiority of the developed MRIME for the TWO-DM of the R.T.C. France cell. Consequently, the suggested MRIME yielded the highest value, indicating that MRIME outperforms RIME in terms of stability, accuracy, and efficacy when determining TWO-DM parameters through comparison. It is reliable that the MRIME identified the validity with the TWO-DM.

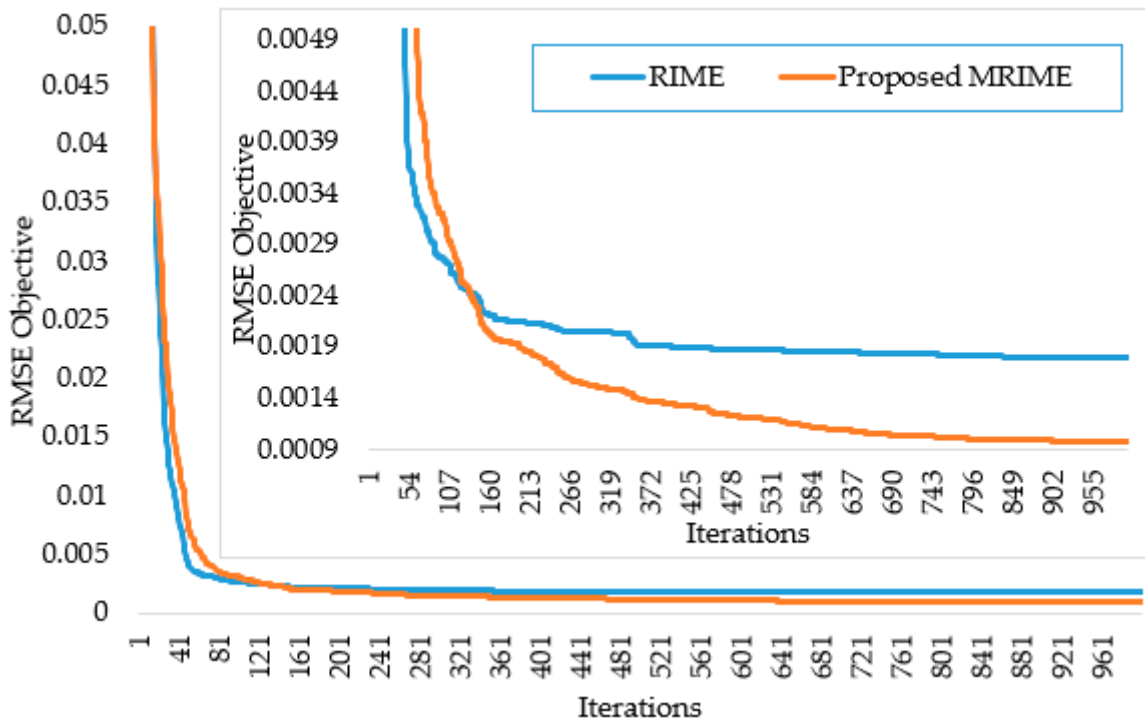


Figure 8. Convergence lines of RIME and MRIME for the TWO-DM of the R.T.C. France cell.

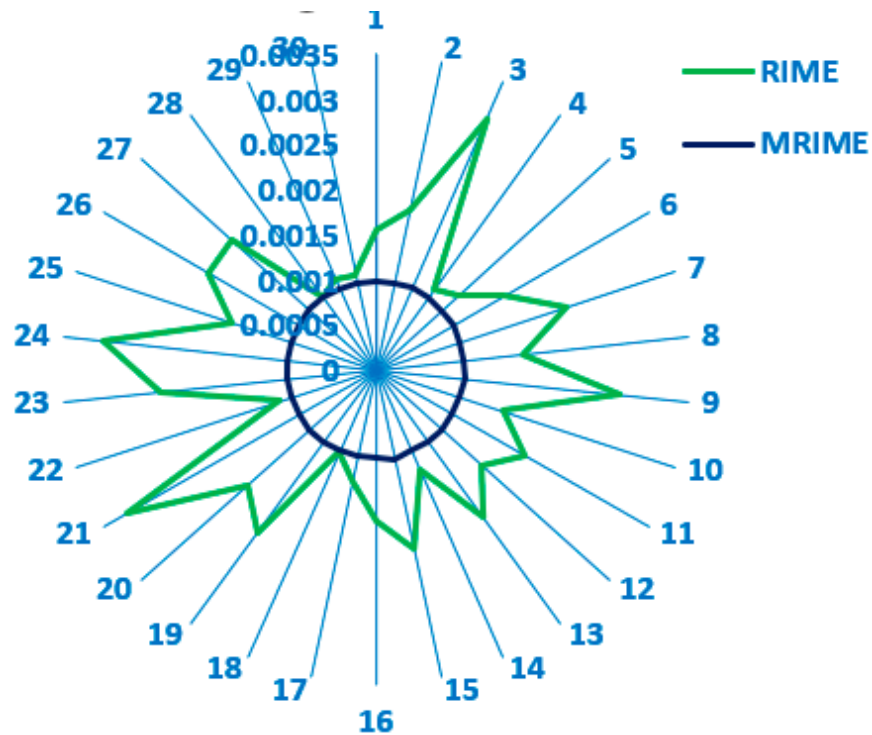


Figure 9. RIME and MRIME of the thirty obtained RMSE objectives for the TWO-DM of the R.T.C. France cell.

For the TWO-DM, the simulated and measured I-V and P-V characteristics are shown in Figure 10a,b. It can be proven that the data created by the MRIME technique are almost the same as the data obtained through experimentation, indicating that the MRIME technique proved effective in obtaining the power and current with diverse voltage levels. As seen from Figure 10a,b, the absolute errors between the simulated and measured currents

are between 2.34255×10^{-9} and 6.33737×10^{-6} , whereas the absolute errors between the simulated and measured powers are between 1.93966×10^{-6} and 1.4684×10^{-3} . In Figures 6 and 10, negative values of voltage, current, and power indicate specific conditions of reverse bias situations. Therefore, based on the experimental study provided by [63], the polarity of the voltage applied to the module is opposite to its normal operating polarity.

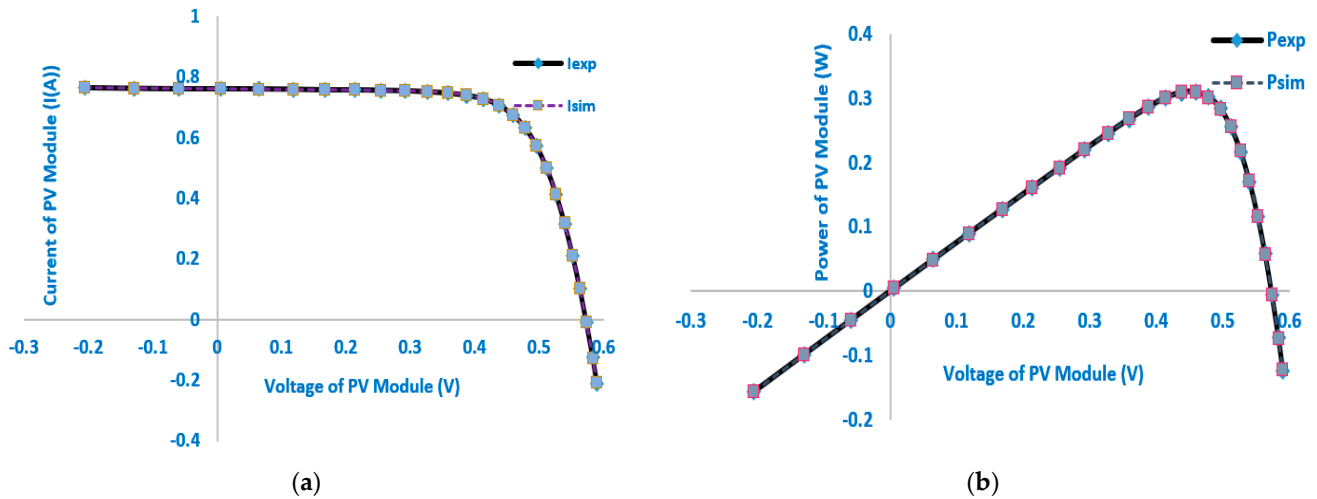


Figure 10. (a) I-V and (b) P-V characteristics of the proposed MRIME for the TWO-DM of the R.T.C. France cell.

4.2. Simulation Results for STM6_40/36 PV Module

4.2.1. Case 1: ONE-DM

In the current case, the ONE-DM characteristics of the STM6_40/36 PV module are extracted using the suggested MRIME and the RIME. Table 4 lists the five unknown ONE-DM parameters for which the experiment’s best outcomes were obtained for every approach. The results show that the suggested MRIME outperforms the RIME and comparator approaches in terms of competitiveness. This means that the regular RIME obtained an RMSE of 2.1693×10^{-3} , whereas the MRIME obtained the best RMSE value of 1.7690×10^{-3} . Additionally, the PV-derived electrical parameters utilizing the reported optimization approaches are displayed in the table, such as Enhanced MPA (EMPA) [47], Simulated Annealing (SA) [64], equilibrium optimizer (EO) [47], improved shuffled complex evolution (ISCE) [65], gorilla troops optimization (GTO) [47], hybridizing cuckoo search/biogeography-based optimization (BHCS) [63], Marine Predator Algorithm (MPA) [47], Jellyfish Search (JFS) [47], three-point based approach (TPBA) [66], heap-based algorithm (HBA) [47], forensic-based investigation (FBI) [53], and improved cuckoo search (ImCSA) algorithm [67]. Moreover, the table specifies the assessed parameters of (MRIME and RIME), which are (17.86858 Ω and 16.80129 Ω), (1.663482 A and 1.663482 A), (1.537805 and 1.5074212), (0.003772 Ω and 0.004785 Ω), and (2.04 μ A and 1.55 μ A) for the shunt resistance, photo-current, ideality factor for d1, series resistance, and saturation current for d1, respectively. Additionally, electrical variables acquired using various inspirational optimizers are expressed in this table. The corresponding convergence lines can be seen in Figure 11. The MRIME converged extremely quickly in the first 60 iterations, as depicted in this figure, demonstrating the MRIME’s excellent convergence capacity. Additionally, Figure 12 shows the thirty obtained RMSE objectives for Case 1’s RIME and MRIME. This figure illustrates that the RMSE of RIME is between $[2.1693 \times 10^{-3}$ and $3.0364 \times 10^{-2}]$, but the RMSE of MRIME is between $[1.7690 \times 10^{-3}$ and $2.2155 \times 10^{-3}]$. It can be established from the figure that the enhancements of the MRIME approach are 85.3678%, 18.4506%, 92.7036%, and 98.9158%, respectively, when compared to the mean, best, worst, and standard deviation of the outcomes of the RIME techniques. These results corroborate the superiority of the developed MRIME for the ONE-DM of the STM6_40/36 PV module. Consequently, the suggested MRIME yielded the highest

value, indicating that MRIME outperforms RIME in terms of stability, accuracy, and efficacy when determining ONE-DM parameters through comparison. It is reliable that the MRIME identified the validity with the ONE-DM of the STM6_40/36 PV module.

Table 4. Electrical parameters accomplished by the proposed MRIME and the standard RIME for the ONE-DM of STM6_40/36.

Algorithm	I_{ph} (A)	I_{S1} (μ A)	R_s (Ω)	R_{sh} (Ω)	η_1	RMSE
MRIME	1.663482	2.04	0.003772	16.80129	1.537805	1.7690×10^{-3}
RIME	1.663482	1.55	0.004785	17.86858	1.5074212	2.1693×10^{-3}
BHCS [63]	1.6639	1.74	0.00427	15.9283	1.5203	1.73×10^{-3}
MPA [47]	1.65702	2.46	0.003831	31.50673	1.559041	3.496×10^{-3}
EO [47]	1.663629	1.78	0.004205	16.24408	1.523146	1.733×10^{-3}
JFS [47]	1.662589	1.84	0.004105	16.96607	1.526795	1.807×10^{-3}
SA [64]	1.6609	5.90	0.0049499	26.7742	1.66602	3.399×10^{-3}
EMPA [47]	1.663418	2.03	0.003788	16.878	1.537713	1.769×10^{-3}
ImCSA [67]	1.663971	2	0.002914	15.84051	1.5335	1.794×10^{-3}
ISCE [65]	1.66390478	1.74	0.004274	15.9283	1.5203	1.73×10^{-3}
HBA [47]	1.661527	5.51	0.00001	23.6426	1.658694	3.33×10^{-3}
GTO [47]	1.663905	1.74	0.004274	15.92829	1.520303	1.73×10^{-3}
FBI [53]	1.66391	1.74	0.004281	15.91743	1.520073	1.73×10^{-3}
TPBA [66]	1.6632	2.77	0.004186	16.7328	1.5656	1.774×10^{-3}

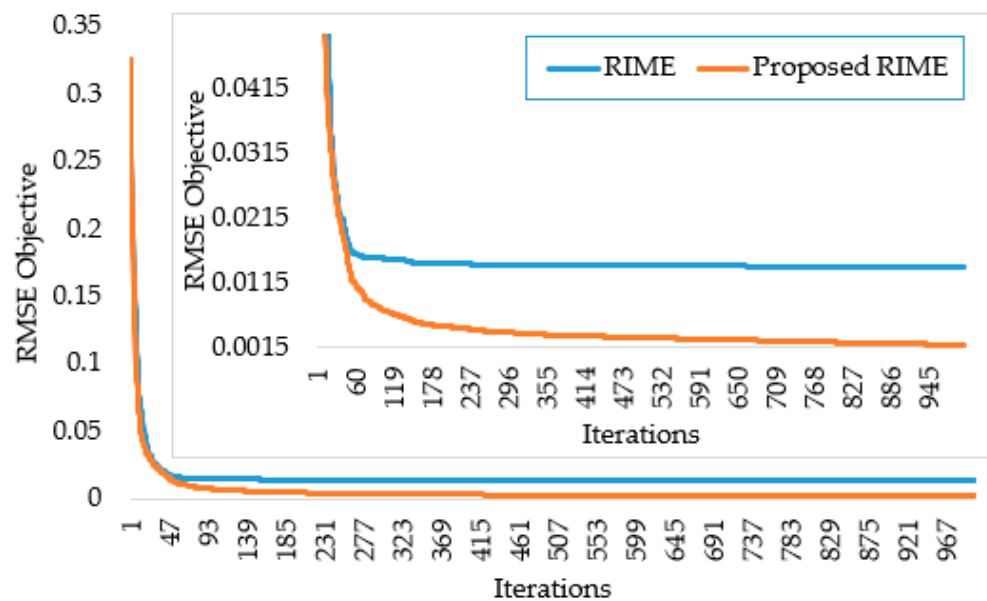


Figure 11. Convergence lines of RIME and MRIME for the ONE-DM of the STM6_40/36 PV module.

For the ONE-DM, the simulated and measured I-V and P-V characteristics are shown in Figure 13a,b. It can be proven that the data created by the MRIME technique are almost the same as the data obtained through experimentation, indicating that the MRIME technique proved effective in obtaining the power and current with diverse voltage levels. As illustrated in Figure 13, the absolute errors between the simulated and measured currents are between 3.58408×10^{-9} and 3.4662×10^{-5} , whereas the absolute errors between the simulated and measured powers are between 0 and 8.7605×10^{-2} .

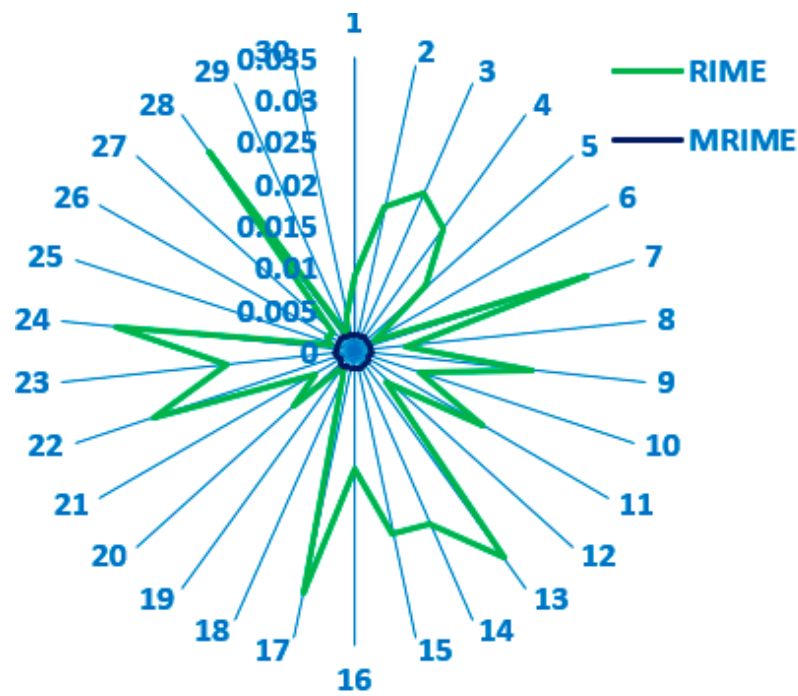


Figure 12. RIME and MRIME of the thirty obtained RMSE objectives for the ONE-DM of the STM6-40/36 PV module.

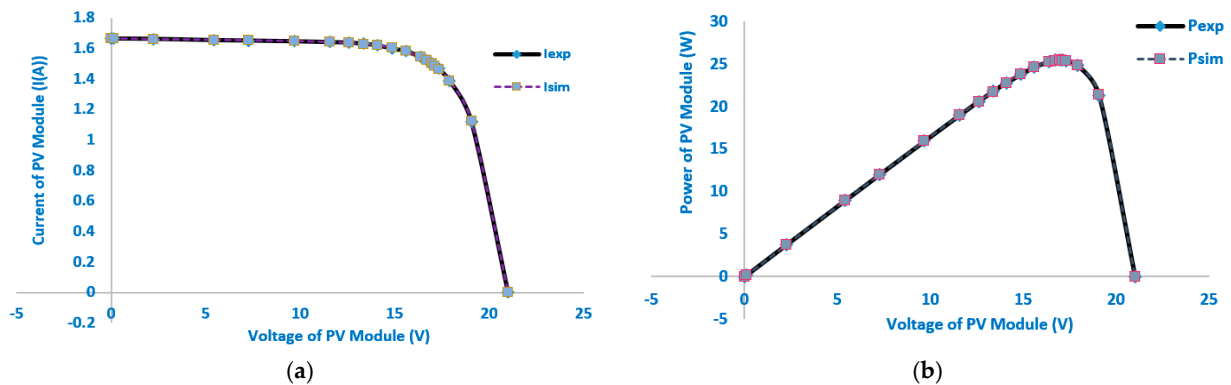


Figure 13. (a) I-V and (b) P-V characteristics of the proposed MRIME for the ONE-DM of the STM6-40/36 PV module.

4.2.2. Case 2: TWO-DM of STM6_40/36 PV Module

In the current case, the characteristics of the STM6-40/36 PV module are extracted using the suggested MRIME and the RIME. Table 5 lists the seven unknown TWO-DM parameters for which the experiment’s best outcomes were obtained for every approach. The results show that the suggested MRIME outperforms the RIME and comparator approaches in terms of competitiveness. This means that the regular RIME obtained an RMSE of 1.9468×10^{-3} , whereas the MRIME obtained the best RMSE value of 1.6988×10^{-3} . Additionally, the PV-derived electrical parameters utilizing the reported optimization approaches are displayed in the table, such as the ensemble particle swarm optimizer (EPSO) [68], improved Rao-based chaotic optimization (LCROA) [69], bat algorithm (BA) [21], directional bat algorithm (DBA) [70], novel bat algorithm (NBA) [70], and fractional chaotic-ensemble particle swarm optimizer (FC-EPSO) algorithm [71]. Moreover, the table specifies the assessed parameters of (MRIME and RIME), which are (17.04779 Ω and 14.54013 Ω), (1.66375 A and 1.666086 A), (1.876731 and 2), (1.361409 and 1.363856), (0.005601 Ω and 0.006291 Ω), (6.007 μ A and 7.509 μ A), and (2.61×10^{-1} μ A and 3.01×10^{-1} μ A) for the shunt resistance, photo-current, ideality factor for d1, ideality factor for d2, series resistance,

saturation current for d1, and saturation current for d2, respectively. Additionally, electrical variables acquired using various inspirational optimizers are expressed in this table.

Table 5. Electrical parameters accomplished by the proposed MRIME and the standard RIME for the TWO-DM of STM6_40/36.

Algorithm	I_{ph} (A)	I_{S1} (μ A)	I_{S2} (μ A)	R_s (Ω)	R_{sh} (Ω)	η_1	η_2	RMSE
MRIME	1.66375	6.007	2.61×10^{-1}	0.005601	17.04779	1.876731	1.361409	1.6988×10^{-3}
RIME	1.666086	7.509	3.01×10^{-1}	0.006291	14.54013	2	1.363856	1.9468×10^{-3}
BA [70]	1.637941	1.59	3.94×10^{-5}	0.003887	24.6958	1.504536	1.4783	2.194577×10^{-2}
EPSO [68]	1.6648	16.70	6.21×10^{-6}	0.5000	16.858	1.16649	1.87067	1.8307×10^{-3}
HPO	1.663702	4.06	5.57×10^{-10}	0.008726	17.82614	1.688851	1	1.696271×10^{-3}
LCROA [69]	1.6637	72.2	3.28×10^{-6}	0.16717	16.7419	1.5739	2.000	1.712×10^{-3}
NBA [70]	1.662865	6.60	1.61×10^{-6}	0.004653	16.694049	1.678806	1.511867	1.82684×10^{-3}
FC-EPPO [71]	1.6634	1.85	9.72×10^{-5}	0.01101	16.5914	1.5818	1.5445	1.772×10^{-3}
DBA [70]	1.663860	1.80	3.66×10^{-6}	0.004167	16.066503	1.524098	1.43939	1.731960×10^{-3}

The corresponding convergence lines can be seen in Figure 14. The MRIME converged extremely quickly in the first 45 iterations, as depicted in this figure, demonstrating the MRIME’s excellent convergence capacity. Additionally, Figure 15 shows the thirty obtained RMSE objectives for Case 2’s RIME and MRIME. This figure illustrates that the RMSE of RIME is between [1.9468×10^{-3} and 8.1478×10^{-3}], but the RMSE of MRIME is between [1.6988×10^{-3} and 2.7435×10^{-3}]. It can be established from the figure that the enhancements of the MRIME approach are 50.4215%, 12.7368%, 66.3287%, 76.9046%, and 99.634%, respectively, when compared to the mean, best, worst, and standard deviation of the outcomes of the RIME techniques. These results corroborate the superiority of the developed MRIME for the TWO-DM of the STM6_40/36 PV module. Consequently, the suggested MRIME yielded the highest value, indicating that MRIME outperforms RIME in terms of stability, accuracy, and efficacy when determining TWO-DM parameters through comparison. It is reliable that the MRIME identified the validity with the TWO-DM of the STM6_40/36 PV module.

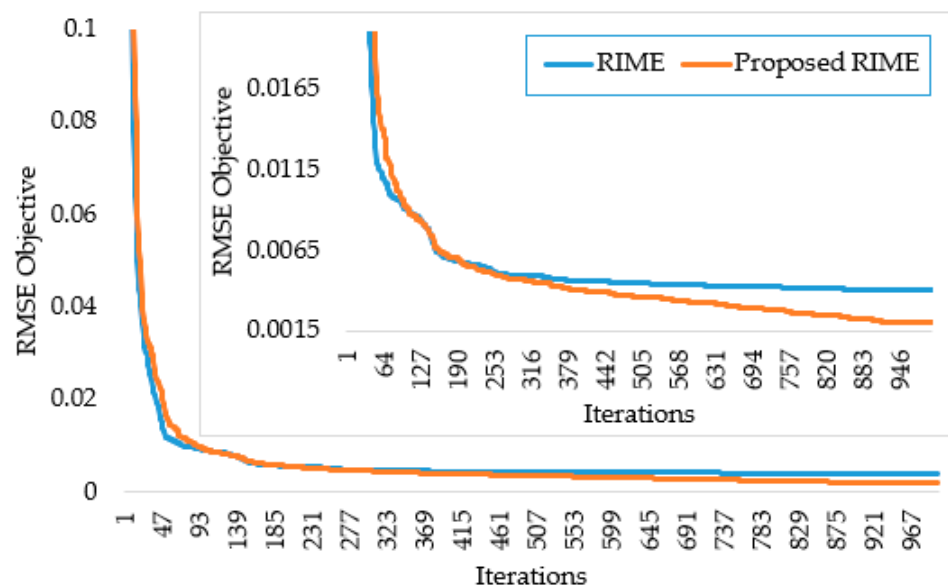


Figure 14. Convergence lines of RIME and MRIME for the TWO-DM of the STM6_40/36 PV module.

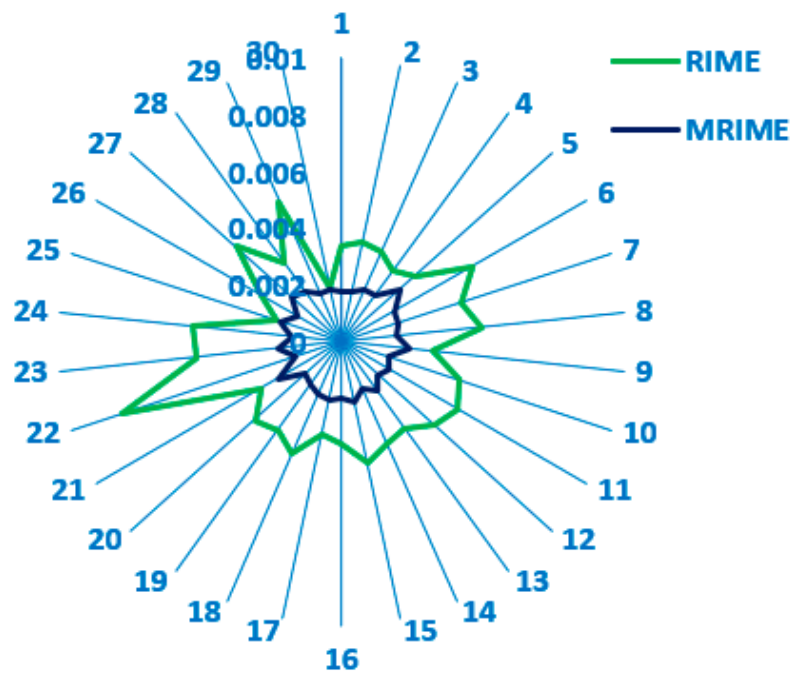


Figure 15. RIME and MRIME of the thirty obtained RMSE objectives for the TWO-DM of the STM6-40/36 PV module.

Additionally, Table 6 presents the statistical analysis and the percentage of improvement of the statistical analysis comparing the efficacy of the proposed MRIME approach to that of the standard RIME, EPSO [68], BA [70], FC-EPSO [71], LCROA [69], DBA [70], and NBA [70]. The results demonstrate that the suggested HPO approach outperforms reported optimizers in terms of overall capability. The minimum, standard deviation (SD), maximum, and mean of the RMSE are successfully attained by the suggested HPO technique, with 1.6988×10^{-3} , 2.0308×10^{-3} , 2.7435×10^{-3} , and 2.6355×10^{-4} , respectively.

Table 6. Statistical analysis of MRIME versus other techniques for the TWO-DM of the STM6-40/36 PV module.

Algorithm	Min.	Improvement %	Mean	Improvement %	Max.	Improvement %	SD	Improvement %
MRIME	1.6988×10^{-3}		2.0308×10^{-3}		2.7435×10^{-3}		2.6355×10^{-4}	
RIME	1.9468×10^{-3}	12.7368%	4.0962×10^{-3}	50.4215%	8.1478×10^{-3}	66.3287%	1.1411×10^{-3}	76.9046%
BA [70]	2.1946×10^{-2}	92.2591%	0.092023	97.7931%	0.01448059	81.0541%	2.407×10^{-2}	98.9051%
DBA [70]	1.7319×10^{-3}	1.9095%	0.004934	58.8404%	0.01372796	80.0154%	2.893×10^{-3}	90.8902%
NBA [70]	1.8268×10^{-3}	7.0052%	0.0041404	50.9512%	0.007598	63.8922%	1.430×10^{-3}	81.5703%
LCROA [69]	1.712×10^{-3}	0.7694%	-	-	-	-	-	-
FC-EPSO [71]	1.772×10^{-3}	4.1293%	-	-	-	-	-	-
EPSO [68]	1.8307×10^{-3}	7.2033%	-	-	-	-	-	-

For the TWO-DM, the simulated and measured I-V and P-V characteristics at the 20 experimental voltage points are shown in Figure 16a,b. It can be proven that the data created by the MRIME technique are almost the same as the data obtained through experimentation, indicating that the MRIME technique proved effective in obtaining the power and current with diverse voltage levels. As illustrated in Table 7 and Figure 17a,b, the absolute errors between the simulated and measured currents are between 5.09971×10^{-9} and 2.5773×10^{-5} , whereas the absolute errors between the simulated and measured powers are between 0 and 7.5541×10^{-2} .

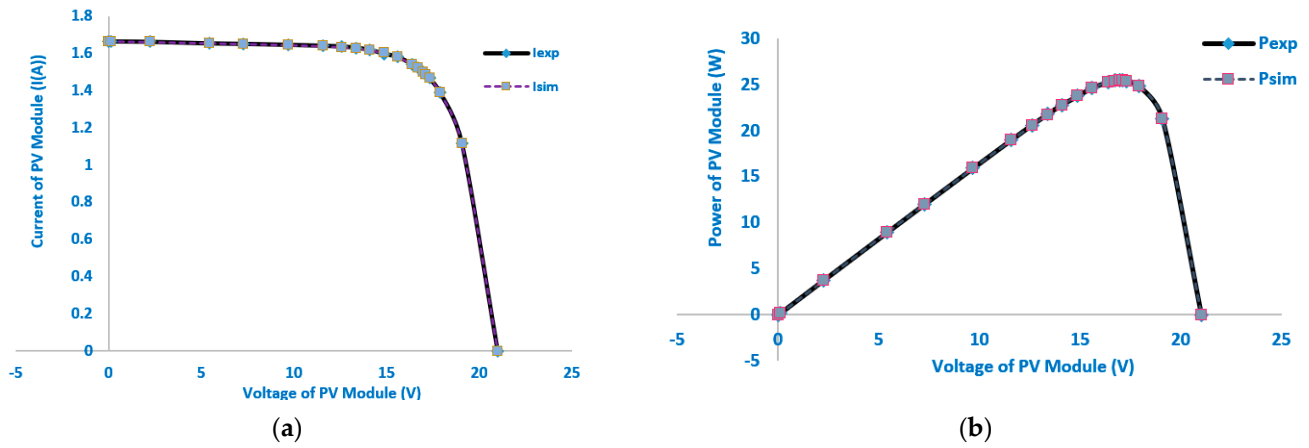


Figure 16. (a) I-V and (b) P-V characteristics of the proposed MRIME for the TWO-DM of the STM6-40/36 PV module.

Table 7. Simulated and experimental currents and powers and the absolute errors established by the proposed MRIME technique for the TWO-DM of the STM6-40/36 PV module.

Point	Vexp	Iexp	Isim	Pexp	Psim	Absolut IAE	Absolut PAE
1	0	1.663	1.665365	0	0	5.59422×10^{-6}	0
2	0.118	1.663	1.665139	0.196234	0.196486	4.57617×10^{-6}	0.000252425
3	2.237	1.661	1.661072	3.715657	3.715819	5.2353×10^{-9}	0.000161859
4	5.434	1.653	1.654842	8.982402	8.992412	3.39332×10^{-6}	0.010009956
5	7.26	1.65	1.651098	11.979	11.98697	1.20484×10^{-6}	0.007968949
6	9.68	1.645	1.645317	15.9236	15.92667	1.0071×10^{-7}	0.003071927
7	11.59	1.64	1.63852	19.0076	18.99044	2.19143×10^{-6}	0.017157251
8	12.6	1.636	1.632709	20.6136	20.57213	1.08307×10^{-5}	0.041466645
9	13.37	1.629	1.626133	21.77973	21.7414	8.2178×10^{-6}	0.038327374
10	14.09	1.619	1.617132	22.81171	22.78539	3.489×10^{-6}	0.026318517
11	14.88	1.597	1.602077	23.76336	23.8389	2.57728×10^{-5}	0.075541147
12	15.59	1.581	1.580929	24.64779	24.64668	5.09971×10^{-9}	0.001113317
13	16.4	1.542	1.54234	25.2888	25.29438	1.15907×10^{-7}	0.005583398
14	16.71	1.524	1.521487	25.46604	25.42404	6.31699×10^{-6}	0.041998279
15	16.98	1.5	1.499757	25.47	25.46588	5.89769×10^{-8}	0.004123622
16	17.13	1.485	1.485979	25.43805	25.45483	9.59298×10^{-7}	0.016777767
17	17.32	1.465	1.466515	25.3738	25.40004	2.29464×10^{-6}	0.02623645
18	17.91	1.388	1.388674	24.85908	24.87116	4.54644×10^{-7}	0.012076229
19	19.08	1.118	1.117554	21.33144	21.32292	1.99239×10^{-7}	0.008516583
20	21.02	0	0.000137	0	0.002871	1.86503×10^{-8}	0.002870618

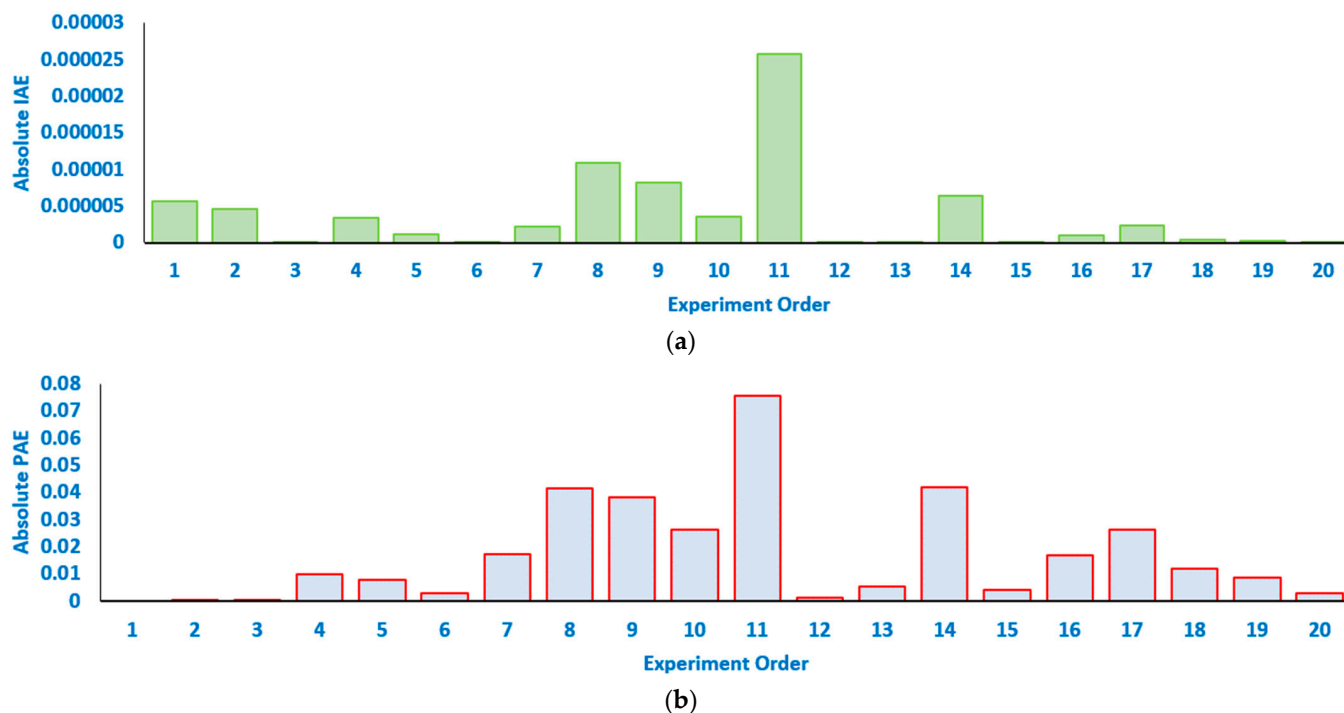


Figure 17. (a,b) The absolute errors between the simulated and measured currents and powers concerning the MRIME for the ONE-DM of the STM6-40/36 PV module.

5. Conclusions

This study introduces the Modified RIME (MRIME) algorithm, an advanced optimization method that integrates the Polynomial Differential Learning Operator (PDLO) with the conventional RIME algorithm. Unlike traditional RIME methods, MRIME incorporates non-linear elements through PDLO, enhancing its adaptability, convergence rate, and overall search capability. Notably, MRIME addresses both the one-diode model (ONE-DM) and TWO-DM, encompassing various equivalent circuit configurations essential for accurately characterizing photovoltaic (PV) modules. Through comprehensive simulations and comparisons with contemporary methods and standard RIME, the MRIME approach demonstrated significant improvements, underscoring its novelty and efficacy in enhancing PV parameter estimation. The enhanced MRIME algorithm was successfully implemented on two commercial PV systems, and both PV models' benefits and robustness were shown to be significantly greater than those of conventional RIME algorithms and prior results. A robust correlation between simulated and real data was found during the MRIME efficacy tests on the PV ONE-DM and TWO-DM, demonstrating the algorithm's performance and dependability. Hence, the MRIME technique is a promising development in PV parameter identification optimization methods.

As future studies, the proposed MRIME algorithm could include sensitivity analysis to certain parameters, computational complexity, or constraints in handling specific types of data or scenarios. Also, the research area could be extended to involve exploring alternative optimization techniques, integrating additional data sources or features, or investigating novel approaches to parameter estimation in photovoltaic systems. Moreover, potential real-world applications and implications of the improved MRIME algorithm could be explored.

Author Contributions: Conceptualization, S.H.H.; Methodology, G.M.; Software, A.M.S.; Validation, A.R.G. and A.M.S.; Formal analysis, H.A.; Investigation, S.H.H.; Data curation, H.A.; Writing—original draft, A.R.G. and A.M.S.; Writing—review & editing, G.M.; Visualization, G.M. and A.R.G. All authors have read and agreed to the published version of the manuscript.

Funding: This research received funding from Ministry of Education in Saudi Arabia.

Data Availability Statement: Data are contained within the article.

Acknowledgments: The authors extend their appreciation to the Deputyship for Research & Innovation, Ministry of Education in Saudi Arabia, for funding this research work through the project number ISP23-122.

Conflicts of Interest: The authors declare no conflicts of interest.

References

1. El-Dabah, M.A.; El-Sehiemy, R.A.; Hasanien, H.M.; Saad, B. Photovoltaic model parameters identification using Northern Goshawk Optimization algorithm. *Energy* **2023**, *262*, 125522. [\[CrossRef\]](#)
2. Beşkirli, A.; Dağ, İ. Parameter extraction for photovoltaic models with tree seed algorithm. *Energy Rep.* **2023**, *9*, 174–185. [\[CrossRef\]](#)
3. Ebrahimi, S.M.; Salahshour, E.; Malekzadeh, M.; Gordillo, F. Parameters identification of PV solar cells and modules using flexible particle swarm optimization algorithm. *Energy* **2019**, *179*, 358–372. [\[CrossRef\]](#)
4. Chen, X.; Yu, K.; Du, W.; Zhao, W.; Liu, G. Parameters identification of solar cell models using generalized oppositional teaching learning based optimization. *Energy* **2016**, *99*, 170–180. [\[CrossRef\]](#)
5. Rizk-Allah, R.M.; El-Fergany, A.A. Emended heap-based optimizer for characterizing performance of industrial solar generating units using triple-diode model. *Energy* **2021**, *237*, 121561. [\[CrossRef\]](#)
6. Ortiz-Conde, A.; Sánchez, F.J.G.; Muci, J. New method to extract the model parameters of solar cells from the explicit analytic solutions of their illuminated I–V characteristics. *Sol. Energy Mater. Sol. Cells* **2006**, *90*, 352–361. [\[CrossRef\]](#)
7. Easwarakhanthan, T.; Bottin, J.; Bouhouch, I.; Boutrit, C. Nonlinear Minimization Algorithm for Determining the Solar Cell Parameters with Microcomputers. *Int. J. Sol. Energy* **1986**, *4*, 1–12. [\[CrossRef\]](#)
8. Fan, Y.; Wang, P.; Mafarja, M.; Wang, M.; Zhao, X.; Chen, H. A bioinformatic variant fruit fly optimizer for tackling optimization problems. *Knowl.-Based Syst.* **2021**, *213*, 106704. [\[CrossRef\]](#)
9. Ridha, H.M.; Heidari, A.A.; Wang, M.; Chen, H. Boosted mutation-based Harris hawks optimizer for parameters identification of single-diode solar cell models. *Energy Convers. Manag.* **2020**, *209*, 112660. [\[CrossRef\]](#)
10. Chen, H.; Jiao, S.; Wang, M.; Heidari, A.A.; Zhao, X. Parameters identification of photovoltaic cells and modules using diversification-enriched Harris hawks optimization with chaotic drifts. *J. Clean. Prod.* **2020**, *244*, 118778. [\[CrossRef\]](#)
11. Zhang, H.; Heidari, A.A.; Wang, M.; Zhang, L.; Chen, H.; Li, C. Orthogonal Nelder-Mead moth flame method for parameters identification of photovoltaic modules. *Energy Convers. Manag.* **2020**, *211*, 112764. [\[CrossRef\]](#)
12. Chen, H.; Jiao, S.; Heidari, A.A.; Wang, M.; Chen, X.; Zhao, X. An opposition-based sine cosine approach with local search for parameter estimation of photovoltaic models. *Energy Convers. Manag.* **2019**, *195*, 927–942. [\[CrossRef\]](#)
13. Wu, Z.; Yu, D.; Kang, X. Parameter identification of photovoltaic cell model based on improved ant lion optimizer. *Energy Convers. Manag.* **2017**, *151*, 107–115. [\[CrossRef\]](#)
14. Liu, Y.; Chong, G.; Heidari, A.A.; Chen, H.; Liang, G.; Ye, X.; Cai, Z.; Wang, M. Horizontal and vertical crossover of Harris hawk optimizer with Nelder-Mead simplex for parameter estimation of photovoltaic models. *Energy Convers. Manag.* **2020**, *223*, 113211. [\[CrossRef\]](#)
15. Nunes, H.G.G.; Pombo, J.A.N.; Mariano, S.J.P.S.; Calado, M.R.A.; Felipe de Souza, J.A.M. A new high performance method for determining the parameters of PV cells and modules based on guaranteed convergence particle swarm optimization. *Appl. Energy* **2017**, *211*, 774–791. [\[CrossRef\]](#)
16. Merchaoui, M.; Sakly, A.; Mimouni, M.F. Particle swarm optimisation with adaptive mutation strategy for photovoltaic solar cell/module parameter extraction. *Energy Convers. Manag.* **2018**, *175*, 151–163. [\[CrossRef\]](#)
17. Jiao, S.; Chong, G.; Huang, C.; Hu, H.; Wang, M.; Heidari, A.A.; Chen, H.; Zhao, X. Orthogonally adapted Harris hawks optimization for parameter estimation of photovoltaic models. *Energy* **2020**, *203*, 117804. [\[CrossRef\]](#)
18. Abbassi, A.; Abbassi, R.; Heidari, A.A.; Oliva, D.; Chen, H.; Habib, A.; Jemli, M.; Wang, M. Parameters identification of photovoltaic cell models using enhanced exploratory salp chains-based approach. *Energy* **2020**, *198*, 117333. [\[CrossRef\]](#)
19. Ridha, H.M.; Gomes, C.; Hizam, H.; Ahmadipour, M.; Heidari, A.A.; Chen, H. Multi-objective optimization and multi-criteria decision-making methods for optimal design of standalone photovoltaic system: A comprehensive review. *Renew. Sustain. Energy Rev.* **2021**, *135*, 110202. [\[CrossRef\]](#)
20. Smaili, I.H.; Almalawi, D.R.; Shaheen, A.M.; Mansour, H.S.E. Optimizing PV Sources and Shunt Capacitors for Energy Efficiency Improvement in Distribution Systems Using Subtraction-Average Algorithm. *Mathematics* **2024**, *12*, 625. [\[CrossRef\]](#)
21. Alam, M.M.; Alshahrani, T.; Khan, F.; Hakami, J.; Shinde, S.M.; Azim, R. AI-based efficiency analysis technique for photovoltaic renewable energy system. *Phys. Scr.* **2023**, *98*, 126006. [\[CrossRef\]](#)
22. Shaheen, A.M.; El-Sehiemy, R.A.; Ginidi, A.; Elsayed, A.M.; Al-Gahtani, S.F. Optimal Allocation of PV-STATCOM Devices in Distribution Systems for Energy Losses Minimization and Voltage Profile Improvement via Hunter-Prey-Based Algorithm. *Energies* **2023**, *16*, 2790. [\[CrossRef\]](#)
23. Shaheen, A.M.; Elattar, E.E.; Nagem, N.A.; Nasef, A.F. Allocation of PV Systems with Volt/Var Control Based on Automatic Voltage Regulators in Active Distribution Networks. *Sustainability* **2023**, *15*, 15634. [\[CrossRef\]](#)

24. Al-Dhaifallah, M.; Alaas, Z.; Rezvani, A.; Nguyen Le, B.; Samad, S. RETRACTED: Optimal day-ahead economic/emission scheduling of renewable energy resources based microgrid considering demand side management. *J. Build. Eng.* **2023**, *76*, 107070. [[CrossRef](#)]
25. Alaas, Z.; Elbarbary, Z.M.S.; Rezvani, A.; Le, B.N.; khaki, M. Analysis and enhancement of MPPT technique to increase accuracy and speed in photovoltaic systems under different conditions. *Optik* **2023**, *289*, 171208. [[CrossRef](#)]
26. Wang, K.; Ma, J.; Man, K.L.; Huang, K.; Huang, X. Comparative study of modern heuristic algorithms for global maximum power point tracking in photovoltaic systems under partial shading conditions. *Front. Energy Res.* **2022**, *10*, 946864. [[CrossRef](#)]
27. Verma, P.; Alam, A.; Sarwar, A.; Tariq, M.; Vahedi, H.; Gupta, D.; Ahmad, S.; Adamali Shah, N.M. Meta-heuristic optimization techniques used for maximum power point tracking in solar pv system. *Electronics* **2021**, *10*, 2419. [[CrossRef](#)]
28. Nagadurga, T.; Devarapalli, R.; Knypiński, Ł. Comparison of Meta-Heuristic Optimization Algorithms for Global Maximum Power Point Tracking of Partially Shaded Solar Photovoltaic Systems. *Algorithms* **2023**, *16*, 376. [[CrossRef](#)]
29. Su, H.; Zhao, D.; Heidari, A.A.; Liu, L.; Zhang, X.; Mafarja, M.; Chen, H. RIME: A physics-based optimization. *Neurocomputing* **2023**, *532*, 183–214. [[CrossRef](#)]
30. Zhao, K. Stability of a Nonlinear Langevin System of ML-Type Fractional Derivative Affected by Time-Varying Delays and Differential Feedback Control. *Fractal Fract.* **2022**, *6*, 725. [[CrossRef](#)]
31. Zhao, K. Solvability, Approximation and Stability of Periodic Boundary Value Problem for a Nonlinear Hadamard Fractional Differential Equation with p-Laplacian. *Axioms* **2023**, *12*, 733. [[CrossRef](#)]
32. Zhao, K. Study on the stability and its simulation algorithm of a nonlinear impulsive ABC-fractional coupled system with a Laplacian operator via F-contractive mapping. *Adv. Contin. Discret. Model.* **2024**, *2024*, 5. [[CrossRef](#)]
33. Zhao, K.; Liu, J.; Lv, X. A Unified Approach to Solvability and Stability of Multipoint BVPs for Langevin and Sturm–Liouville Equations with CH-Fractional Derivatives and Impulses via Coincidence Theory. *Fractal Fract.* **2024**, *8*, 111. [[CrossRef](#)]
34. Yu, X.; Duan, Y.; Cai, Z. Sub-population improved grey wolf optimizer with Gaussian mutation and Lévy flight for parameters identification of photovoltaic models. *Expert Syst. Appl.* **2023**, *232*, 120827. [[CrossRef](#)]
35. Chin, V.J.; Salam, Z.; Ishaque, K. Cell modelling and model parameters estimation techniques for photovoltaic simulator application: A review. *Appl. Energy* **2015**, *154*, 500–519. [[CrossRef](#)]
36. Shaheen, A.; El-Sehiemy, R.; El-Fergany, A.; Ginidi, A. Representations of solar photovoltaic triple-diode models using artificial hummingbird optimizer. *Energy Sources Part A Recovery Util. Environ. Eff.* **2022**, *44*, 8787–8810. [[CrossRef](#)]
37. Ginidi, A.R.; Shaheen, A.M.; El-Sehiemy, R.A.; Hasanien, H.M.; Al-Durra, A. Estimation of electrical parameters of photovoltaic panels using heap-based algorithm. *IET Renew. Power Gener.* **2022**, *16*, 2292–2312. [[CrossRef](#)]
38. Aribia, H.B.; El-Rifaie, A.M.; Tolba, M.A.; Shaheen, A.; Moustafa, G.; Elsayed, F.; Elshahed, M. Growth Optimizer for Parameter Identification of Solar Photovoltaic Cells and Modules. *Sustainability* **2023**, *15*, 7896. [[CrossRef](#)]
39. Elshahed, M.; El-Rifaie, A.M.; Tolba, M.A.; Ginidi, A.; Shaheen, A.; Mohamed, S.A. An Innovative Hunter-Prey-Based Optimization for Electrically Based Single-, Double-, and Triple-Diode Models of Solar Photovoltaic Systems. *Mathematics* **2022**, *10*, 4625. [[CrossRef](#)]
40. Lu, Y.; Liang, S.; Ouyang, H.; Li, S.; Wang, G.-g. Hybrid multi-group stochastic cooperative particle swarm optimization algorithm and its application to the photovoltaic parameter identification problem. *Energy Rep.* **2023**, *9*, 4654–4681. [[CrossRef](#)]
41. Chin, V.J.; Salam, Z. Coyote optimization algorithm for the parameter extraction of photovoltaic cells. *Sol. Energy* **2019**, *194*, 656–670. [[CrossRef](#)]
42. Moustafa, G.; Alnami, H.; Hakmi, S.H.; Ginidi, A.; Shaheen, A.M.; Al-Mufadi, F.A. An Advanced Bio-Inspired Mantis Search Algorithm for Characterization of PV Panel and Global Optimization of Its Model Parameters. *Biomimetics* **2023**, *8*, 490. [[CrossRef](#)]
43. Moustafa, G.; Smaili, I.H.; Almalawi, D.R.; Ginidi, A.R.; Shaheen, A.M.; Elshahed, M.; Mansour, H.S.E. Dwarf Mongoose Optimizer for Optimal Modeling of Solar PV Systems and Parameter Extraction. *Electronics* **2023**, *12*, 4990. [[CrossRef](#)]
44. Ahmad, M.F.; Isa, N.A.M.; Lim, W.H.; Ang, K.M. Differential evolution: A recent review based on state-of-the-art works. *Alex. Eng. J.* **2022**, *61*, 3831–3872. [[CrossRef](#)]
45. Tong, N.T.; Pora, W. A parameter extraction technique exploiting intrinsic properties of solar cells. *Appl. Energy* **2016**, *176*, 104–115. [[CrossRef](#)]
46. Liang, J.; Ge, S.; Qu, B.; Yu, K.; Liu, F.; Yang, H.; Wei, P.; Li, Z. Classified perturbation mutation based particle swarm optimization algorithm for parameters extraction of photovoltaic models. *Energy Convers. Manag.* **2020**, *203*, 112138. [[CrossRef](#)]
47. Ginidi, A.; Ghoneim, S.M.; Elsayed, A.; El-Sehiemy, R.; Shaheen, A.; El-Fergany, A. Gorilla Troops Optimizer for Electrically Based Single and Double-Diode Models of Solar Photovoltaic Systems. *Sustainability* **2021**, *13*, 9459. [[CrossRef](#)]
48. Ali, E.E.; El-Hameed, M.A.; El-Fergany, A.A.; El-Arini, M.M. Parameter extraction of photovoltaic generating units using multi-verse optimizer. *Sustain. Energy Technol. Assess.* **2016**, *17*, 68–76. [[CrossRef](#)]
49. Nematollahi, A.F.; Rahiminejad, A.; Vahidi, B. A novel physical based meta-heuristic optimization method known as Lightning Attachment Procedure Optimization. *Appl. Soft Comput. J.* **2017**, *59*, 596–621. [[CrossRef](#)]
50. Khanna, V.; Das, B.K.; Bisht, D.; Vandana; Singh, P.K. A three diode model for industrial solar cells and estimation of solar cell parameters using PSO algorithm. *Renew. Energy* **2015**, *78*, 105–113. [[CrossRef](#)]
51. Rizk-Allah, R.M.; El-Fergany, A.A. Conscious neighborhood scheme-based Laplacian barnacles mating algorithm for parameters optimization of photovoltaic single- and double-diode models. *Energy Convers. Manag.* **2020**, *226*, 113522. [[CrossRef](#)]

52. Yu, K.; Qu, B.; Yue, C.; Ge, S.; Chen, X.; Liang, J. A performance-guided JAYA algorithm for parameters identification of photovoltaic cell and module. *Appl. Energy* **2019**, *237*, 241–257. [[CrossRef](#)]
53. Shaheen, A.M.; Ginidi, A.R.; El-Sehiemy, R.A.; Ghoneim, S.S.M. A Forensic-Based Investigation Algorithm for Parameter Extraction of Solar Cell Models. *IEEE Access* **2021**, *9*, 1–20. [[CrossRef](#)]
54. Sulaiman, M.H.; Mustaffa, Z.; Saari, M.M.; Daniyal, H. Barnacles Mating Optimizer: A new bio-inspired algorithm for solving engineering optimization problems. *Eng. Appl. Artif. Intell.* **2020**, *87*, 103330. [[CrossRef](#)]
55. Kanimozhi, G.; Kumar, H. Modeling of solar cell under different conditions by Ant Lion Optimizer with LambertW function. *Appl. Soft Comput. J.* **2018**, *71*, 141–151. [[CrossRef](#)]
56. Beigi, A.M.; Maroosi, A. Parameter identification for solar cells and module using a Hybrid Firefly and Pattern Search Algorithms. *Sol. Energy* **2018**, *171*, 435–446. [[CrossRef](#)]
57. Şenel, F.A.; Gökçe, F.; Yüksel, A.S.; Yiğit, T. A novel hybrid PSO–GWO algorithm for optimization problems. *Eng. Comput.* **2019**, *35*, 1359–1373. [[CrossRef](#)]
58. Xu, S.; Wang, Y. Parameter estimation of photovoltaic modules using a hybrid flower pollination algorithm. *Energy Convers. Manag.* **2017**, *144*, 53–68. [[CrossRef](#)]
59. Chen, X.; Xu, B.; Mei, C.; Ding, Y.; Li, K. Teaching–learning–based artificial bee colony for solar photovoltaic parameter estimation. *Appl. Energy* **2018**, *212*, 1578–1588. [[CrossRef](#)]
60. Rao, R.V.; Savsani, V.J.; Vakharia, D.P. Teaching—Learning-based optimization: An optimization method for continuous non-linear large scale problems. *Inf. Sci.* **2012**, *183*, 1–15. [[CrossRef](#)]
61. Oliva, D.; Cuevas, E.; Pajares, G. Parameter identification of solar cells using artificial bee colony optimization. *Energy* **2014**, *72*, 93–102. [[CrossRef](#)]
62. Guo, L.; Meng, Z.; Sun, Y.; Wang, L. Parameter identification and sensitivity analysis of solar cell models with cat swarm optimization algorithm. *Energy Convers. Manag.* **2016**, *108*, 520–528. [[CrossRef](#)]
63. Chen, X.; Yu, K. Hybridizing cuckoo search algorithm with biogeography-based optimization for estimating photovoltaic model parameters. *Sol. Energy* **2019**, *180*, 192–206. [[CrossRef](#)]
64. Ben Messaoud, R. Extraction of uncertain parameters of a single-diode model for a photovoltaic panel using lightning attachment procedure optimization. *J. Comput. Electron.* **2020**, *19*, 1192–1202. [[CrossRef](#)]
65. Gao, X.; Cui, Y.; Hu, J.; Xu, G.; Wang, Z.; Qu, J.; Wang, H. Parameter extraction of solar cell models using improved shuffled complex evolution algorithm. *Energy Convers. Manag.* **2018**, *157*, 460–479. [[CrossRef](#)]
66. Chin, V.J.; Salam, Z. A New Three-point-based Approach for the Parameter Extraction of Photovoltaic Cells. *Appl. Energy* **2019**, *237*, 519–533. [[CrossRef](#)]
67. Kang, T.; Yao, J.; Jin, M.; Yang, S.; Duong, T. A novel improved cuckoo search algorithm for parameter estimation of photovoltaic (PV) models. *Energies* **2018**, *11*, 1060. [[CrossRef](#)]
68. Rezaee Jordehi, A. Enhanced leader particle swarm optimisation (ELPSO): An efficient algorithm for parameter estimation of photovoltaic (PV) cells and modules. *Sol. Energy* **2018**, *159*, 78–87. [[CrossRef](#)]
69. Lekouaghet, B.; Boukabou, A.; Boubakir, C. Estimation of the photovoltaic cells/modules parameters using an improved Rao-based chaotic optimization technique. *Energy Convers. Manag.* **2021**, *229*, 113722. [[CrossRef](#)]
70. Deotti, L.M.P.; Pereira, J.L.R.; da Silva Junior, I.C. Parameter extraction of photovoltaic models using an enhanced Lévy flight bat algorithm. *Energy Convers. Manag.* **2020**, *221*, 113114. [[CrossRef](#)]
71. Yousri, D.; Thanikanti, S.B.; Allam, D.; Ramachandaramurthy, V.K.; Eteiba, M.B. Fractional chaotic ensemble particle swarm optimizer for identifying the single, double, and three diode photovoltaic models' parameters. *Energy* **2020**, *195*, 116979. [[CrossRef](#)]

Disclaimer/Publisher's Note: The statements, opinions and data contained in all publications are solely those of the individual author(s) and contributor(s) and not of MDPI and/or the editor(s). MDPI and/or the editor(s) disclaim responsibility for any injury to people or property resulting from any ideas, methods, instructions or products referred to in the content.